Thermal treatment of electrodes for Flow Battery Applications

Master's Thesis

Submitted by:

Youssef Sayed, B.Sc.

Supervised by:

Antonio Rodolfo dos Santos, PhD

Department of Research and Development, VoltStorage GmbH

July 14th, 2023

This page is intentionally left blank.

TABLE OF CONTENTS

LIST OF ABBREVIATIONS AND SYMBOLS

I_a	Anodic current peak	PAN	PAN-based graphite felt
E_a	Anodic potential peak	ΔE_p	Potential peak separation
BPP	Bipolar plate	Rayon	Rayon-based graphite felt
I_c	**C**athodic current peak	FBs	Flow batteries
E_c	Cathodic potential peak	SOC	State-of-charge
CE	Coulombic efficiency	TGA	**T**hermogravimetric analysis
CV	Cyclic voltammetry	VFB	Vanadium flow battery
CCC	Copper current collector	VE	Voltaic efficiency
EIS	Electrochemical impedance spectroscopy	C/D	Charge/discharge
EE	Energy efficiency	XPS	X-ray photoelectron spectroscopy
ESSs	Energy storage systems		
OCV	Open-circuit voltage		

ACKNOWLEDGEMENTS

I would like to take this opportunity to express my heartfelt gratitude to all those who have supported and contributed to the completion of my master's thesis. Their guidance, encouragement, and assistance have been instrumental in shaping the outcome of this research endeavor.

First and foremost, I am deeply indebted to Antonio, my supervisor at VoltStorage, for his invaluable assistance throughout my internship. His unwavering support, receptiveness to my ideas and feedback, and willingness to share his technical expertise and theoretical knowledge have been instrumental in shaping my research. I am grateful to Nicolas for his guidance and continuous feedback on my experimental work, documentation, and data analysis. His insights and expertise have been immensely valuable in enhancing the quality of my research. I would like to acknowledge Ary for his unwavering support and encouragement during moments of disappointment arising from negative results. His ability to lighten the atmosphere in the lab with his spontaneous jokes and infectious smile greatly alleviated any stress and motivated me to persist in my work.

I would like to express my gratitude to Alexandra for her dynamic presence and infectious energy that invigorated the entire office, creating a positive and productive environment each morning. Special thanks go to John for his invaluable feedback during presentations and his diligent follow-up on the progress of the project. Also, deep thanks go to Charlotte for the thought-provoking conversations we had on a wide range of topics. Her unique perspectives and insights have broadened my horizons and challenged me to think beyond the conventional boundaries. Charlotte’s ability to balance work, studies, and sports with such finesse has been an inspiration to me. I would like to thank Julia, Pablo, and all the other members of the R&D team at VoltStorage for their support, cooperation, and valuable contributions to my research. Their collaboration and expertise have significantly enriched my learning experience. I am grateful to the entire VoltStorage team for making me feel like a part of their community, embracing me with open arms, and providing a conducive environment for personal and professional growth.

I am indebted to the coordinators, staff, and faculty of SERP Program for providing a conducive academic environment and access to necessary resources, which facilitated the smooth progress of my research. Their commitment to academic excellence has been a constant source of inspiration. I extend special thanks to Prof. Sandrine, Prof. Rocca, and Prof. Eduardo Marques for his continuous mentorship during the internship selection process. Their guidance and expertise have been invaluable in shaping my academic and professional development. Thanks, Eva, for your continuous patience, help, consideration, prompt responses, and detailed answers to my queries. Your role in resolving any urgent situations that arose during my research was truly indispensable.

I am grateful to my colleagues and friends for their encouragement, valuable discussions, and support during my master study. Their intellectual stimulation and camaraderie have made this journey more enjoyable and rewarding. I would also like to express my deep appreciation to my family for their unwavering support, understanding, and encouragement throughout my academic pursuits. Their love, patience, and belief in my abilities have been a constant source of motivation.

Lastly, I would like to acknowledge the countless individuals, both known and unknown, who have contributed to my personal and academic growth. Their contributions, whether direct or indirect, have shaped my perspectives and enriched my learning experience.

In conclusion, this thesis would not have been possible without the collective efforts and contributions of all those mentioned above. I am truly grateful for their support and encouragement, which have been instrumental in the successful completion of this milestone in my academic journey.

ABSTRACT

Vanadium flow batteries (VFBs) offer tremendous potential as cost-effective, durable, versatile, and safe solutions for large-scale stationary energy storage systems. Despite their numerous advantages, further advancements are necessary to enhance their performance for commercialization. Since the electrode's electrochemical activity influences the whole performance of VFBs, research was directed to explore surface modification methods to improve the electrode's surface functionalization. In this regard, this work investigates the effects of thermal treatment on the surface area and wettability of two types of graphite felts (PAN and rayon) used as electrodes in VFBs. The study focuses on enhancing surface activity by introducing more functional groups on the electrode surface. Comprehensive electrochemical measurements, including cyclic voltammetry (CV), electrochemical impedance spectroscopy (EIS), and charge/discharge (C/D) tests, are conducted to analyse the effects of thermal treatment on the electrochemical activities and efficiency of VFBs.

Cyclic voltammetry reveals that thermal treatment increases the electrochemical reversibility, reflected by the improved I_a/I_c ratio (from 2.7 to 0.97) for PAN and (from 2.2 to 1.03) for rayon. Charge-transfer resistance, measured by EIS, is significantly reduced after treatment, reaching 3.23 and 2.1 Ω for PAN and rayon, respectively, compared to 440 and 128 Ω for the untreated samples. The improvements observed in electrochemical activity for both half-reactions can be attributed to the reduction in overpotential, enhancing the battery's overall performance. The C/D of VFB single-cells show enhancements in efficiencies after the thermal treatment. For example, the highest obtained Voltage efficiencies (VEs) are 89% and 84%, corresponding to PAN treated at 600 °C for 1 hour and rayon treated at 450 °C for 3 hours. The findings contribute to developing more efficient and sustainable energy storage systems that can be integrated as renewable energy sources.

RÉSUMÉ

Les batteries à flux de vanadium (VFB) offrent un potentiel énorme en tant que solutions rentables, durables, polyvalentes et sûres pour les systèmes de stockage d'énergie stationnaires à grande échelle. Malgré leurs nombreux avantages, des progrès supplémentaires sont nécessaires pour améliorer leurs performances en vue de leur commercialisation. Étant donné que l'activité électrochimique de l'électrode influence l'ensemble des performances des VFB, la recherche a été orientée vers l'exploration de méthodes de modification de la surface afin d'améliorer la fonctionnalisation de la surface des électrodes. À cet égard, ce travail étudie les effets du traitement thermique sur la surface et la mouillabilité de deux types de feutres de graphite (PAN et rayonne) utilisés comme électrodes dans les VFB. L'étude se concentre sur l'amélioration de l'activité de surface en introduisant davantage de groupes fonctionnels à la surface de l'électrode. Des mesures électrochimiques complètes, comprenant la voltampérométrie cyclique (CV), la spectroscopie d'impédance électrochimique (EIS) et les tests de charge/décharge (C/D), sont effectuées pour analyser les effets du traitement thermique sur les activités électrochimiques et l'efficacité des VFB.

La voltampérométrie cyclique révèle que le traitement thermique augmente la réversibilité électrochimique, comme en témoigne l'amélioration du rapport Ia/Ic (de 2,7 à 0,97) pour le PAN et (de 2,2 à 1,03) pour la rayonne. La résistance au transfert de charge, mesurée par EIS, est significativement réduite après le traitement, atteignant 3,23 et 2,1 Ω pour le PAN et la rayonne, respectivement, contre 440 et 128 Ω pour les échantillons non traités. Les améliorations observées dans l'activité électrochimique pour les deux demi-réactions peuvent être attribuées à la réduction du surpotentiel, améliorant ainsi la performance globale de la batterie. La C/D des piles uniques VFB montre une amélioration des rendements après le traitement thermique. Par exemple, les efficacités de tension (VE) les plus élevées sont de 89% et 84%, correspondant au PAN traité à 600 °C pendant 1 heure et à la rayonne traitée à 450 °C pendant 3 heures. Ces résultats contribuent au développement de systèmes de stockage d'énergie plus efficaces et durables, qui peuvent être intégrés en tant que sources d'énergie renouvelables.

1. INTRODUCTION

In recent times, there has been a substantial increase in the demand for electrical energy due to the industrial revolution and global economic growth. This surge has necessitated exploring non-fossil energy technologies such as geothermal, wind, and solar power. **[1]**. While developing sustainable energy sources offers sustainable and environmentally friendly alternatives, their effectiveness is hindered by the inherent challenges of variability and intermittency **[2]**. These limitations result in fluctuations in electric power generation, rendering them incapable of being dispatched or controlled in accordance with demand requirements. To address these challenges and enhance grid reliability, it is crucial to have large-scale energy storage systems (ESSs) that can respond quickly to match the fluctuations in power generation. Consequently, a diverse array of ESSs has been developed and successfully demonstrated. These include mechanical approaches like pumped-storage hydroelectricity and compressed-air energy storage; electrochemical and chemical methods such as rechargeable lead-acid batteries, lithium-ion batteries, and fuel cells; as well as thermal techniques like sensible heat storage and latent heat storage **[3, 4].**

Among the mentioned ESSs, flow batteries (FBs) possess significant potential to serve as a buffer, effectively bridging the gap between intermittent electricity production and immediate distribution of electric power, thereby meeting customer requirements. FBs represent a class of electrochemical energy storage devices designed to transform chemical energy into electrical energy and vice versa, facilitating controlled discharge when necessary **[2]**. They serve as a viable alternative for addressing the challenges associated with energy consumption and generation. The fundamental structure of an FB typically encompasses external reservoirs dedicated to energy storage, a main cell responsible for energy transformations, and a circulatory system, which connect the electrolyte tank to the main unit cell **[4]**. Compared to solid-state secondary battery systems, FBs offer many advantages, owing to the implementation of liquid electrolytes and externally housed electroactive materials. These advantages encompass remarkable adaptability and flexibility in design, long life cycles, quick response capabilities, elevated safety measures, simplified thermal management, and economical operation and maintenance requirements. The origins of FBs can be traced back to the 1970s, marked by the groundbreaking invention of the Fe/Cr flow battery at NASA (USA). Subsequently, many FB variations, such as V/Fe, V/Ce, and V/V, have been extensively scrutinized and subject to thorough investigation. In the 1980s and 1990s, considerable research was devoted to exploring different redox couples, with a particular focus on vanadium-based systems **[5]**.

The VFB is the most advanced and promising contender within cutting-edge flow battery technologies. Utilizing vanadium species in the positive and negative tanks within the VFB offers a significant advantage in mitigating the problem of cross-contamination through the membrane [3]. Furthermore, any potential capacity degradation can be effectively reversed by periodically mixing the electrolytes from the two half-cells, ensuring the long-term reliability and durability of VFBs. Also, the frequent occurrence of fire accidents involving high-capacity ESSs utilizing lithium-ion batteries has raised safety concerns. In contrast, using vanadium electrolytes in the VFB offers a significant advantage in terms of safety. The vanadium electrolyte, being a non-flammable aqueous solution, can remarkably restrict temperature escalation due to its high heat capacity. Consequently, VFBs eliminate the risks associated with ignition and explosion, providing a safer energy storage solution **[4].**

1.1. The basic operational principles of VFB

Figure 1 shows the operational concept and fundamental configuration of a battery VFB. The VFB comprises two reservoirs containing VO_2^+/VO^{2+} and V^{3+}/V^{2+} electrolytes, with an ion-exchange membrane serving as a separator within the two half-cells **[13]**. The electrodes positioned on either side of the membrane serve as catalytic sites for the electrochemical reactions occurring within the electrolytes. It is worth noting that the electrodes themselves do not actively partake in the redox reactions. As a result, the electrodes demonstrate durability, especially under carefully regulated operational conditions. Also, throughout this study, V(V), V(IV), V(III), and V(II) are utilized to denote VO_2^+, VO^{2+}, V^{3+}, and V^{2+}, respectively, signifying their oxidation states**.**

The discharge process involves the following electrochemical reactions:

Positive electrode reaction:

$$V^{5+} + e \rightarrow V^{4+}$$

$$VO_2^{+} + 2H^{+} + e^{-} \rightarrow VO^{2+} + H_2O \qquad E^0 = 1.0\ V \qquad (1)$$

Negative electrode reaction:

$$V^{2+} \rightarrow V^{3+} + e^{-} \qquad E^0 = 0.26\ V \qquad (2)$$

Overall electrochemical reaction of the cell:

$$VO_2^{+} + 2H^{+} + V^{2+} \rightarrow VO^{2+} + H_2O + V^{3+} \qquad E^0 = 1.26\ V \qquad (3)$$

During charging, as the redox reactions take place, ions migrate across the membrane while electrons flow through an external circuit. There is a continuous transfer of ions between the surfaces of the negative and positive electrodes, facilitated by the positive and negative electrolyte phases and the ion-conducting membrane. This ion exchange plays a crucial role in maintaining charge balance within the system. In the positive electrode of the VFBs, the electrochemical process involves the oxidation of V(IV) to V(V). In contrast, at the negative electrode, the electrochemical reaction entails the reduction of V(III) to V(II). Conversely, during discharge, V(II) within the negative electrolyte is oxidized to V(III), as illustrated in **Equation (2),** while V(V) in the positive electrolyte is reduced to V(IV), as represented by **Equation (1)** **[6].**

As illustrated in **Figure 1**, the charging and discharging mechanisms within a VFB rely on the processes of oxidation and reduction involving distinct vanadium species. Consequently, a VFB single cell shows a standard open-circuit voltage (OCV) of 1.26 V. Under specific conditions, including temperature, pH value, and vanadium ion concentration, the cell voltage (E) can be precisely determined by employing the Nernst equation:

$$E = 1.26\ V + \frac{RT}{F} \ln\left(\frac{[VO^{2+}][V^{3+}]}{[VO_2^{+}][H^{+}]^2[V^{2+}]}\right) \qquad (4)$$

where T, F, and R are the absolute temperature, Faraday constant, and gas constant, respectively **[7]**.

Practically, the actual cell potential during the charging and discharging process is consistently lower than the theoretical cell potential due to internal losses **[8]**. These internal losses, including the ohmic drop (iR drop), concentration and activation overpotential, significantly influence the cell potential. The overall cell potential during operation can be expressed in the following equation:

$$V_{cell} = (E_C - E_A) - \eta_A - \eta_C - iR_{cell} \qquad (5)$$

where V_{cell} is the voltage at which the cell discharges, E_A is the anodic potential, E_C denotes the cathodic potential. η_A, which is called activation overpotential, signifies the energy needed to initiate the transfer of charge between reactants and electrodes. However, the mass transport process can be expressed by the concentration overpotential, η_C. The current density, *i*, is measured in mA/cm², and R_{cell} is the ohmic resistance specific to the electrode's cross-sectional area (Ω.cm²). The resistances of the current collectors, electrodes, the ion-exchange membrane contributes to the ohmic resistance.

Figure 2 illustrates the cell's voltage and energy efficiency losses during one charge/discharge (C/D) cycle. The diagram provides a breakdown of the cycle, highlighting different regions. Region 1 represents the initial stage of charge and discharge, characterized by the ohmic and activation losses within the cell. Cells with lower losses exhibit lower initial charge voltages and higher discharge voltages, indicating improved performance. Region 2 demonstrates a smooth voltage change where the concentration of vanadium ions in the electrolyte plays a dominant role. In Region 3, a sharp voltage changes towards the end of the C/D process due to mass transport limitations **[1].**

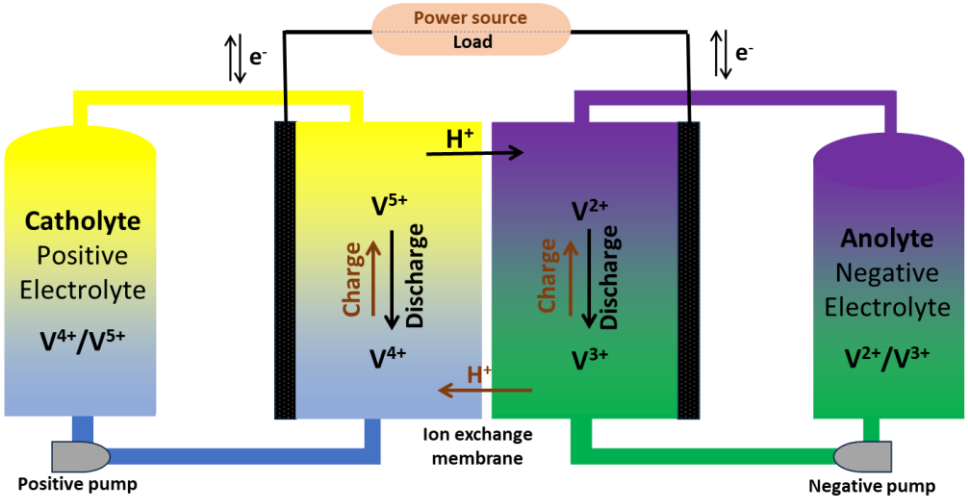

Figure 1: A schematic representation of the vanadium flow battery design.

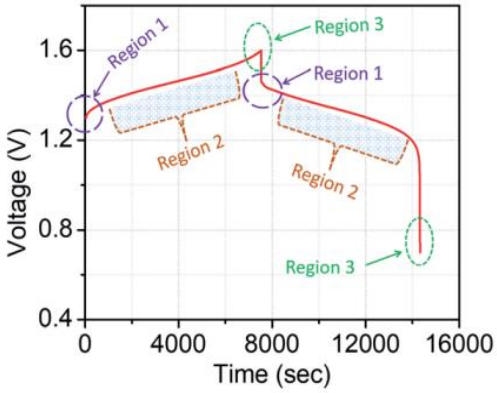

Figure 2: The division of the voltage profile, obtained from the charge-discharge test, into distinct regions **[1].**

1.2. Carbon-based electrode materials of VFB

Electrodes play a crucial role in determining the performance of VFB as they represent the reaction sites. Thus, meeting certain requirements is essential for electrode materials to maintain the battery efficiency, including high electrical conductivity, electrocatalytic activity toward the vanadium ion species, large surface area, mechanical durability during operation, and electrochemical stability. VFBs operate in acidic and corrosive environments, which limits the selection of electrode materials. However, carbon-based materials, such as carbon felt, carbon paper, and graphite felt derived from rayon and polyacrylonitrile (PAN) precursors, are widely utilized in VFBs due to their favourable characteristics such as a wide operation range, low cost, high conductivity, their porous structure, providing large surface area **[9]**.

The choice of the electrode's precursor materials profoundly impacts the performance of graphite felts in VFBs. For example, a previous study has revealed variations in the electrochemical properties between rayon-based (rayon) and PAN-based (PAN) graphite felts. Specifically, the PAN graphite felts exhibited better electrical conductivity and resistance to oxidation compared to the rayon felts. On the other hand, rayon felts are characterized by their reactivity towards oxygen, forming carbon-oxygen functional groups, which make it more feasible for oxidation **[8]**. This is because the chemical composition and structure of rayon graphite felts contribute to their heightened reactivity towards oxygen. Rayon, which is derived from cellulose, contains a notable concentration of hydroxyl (-OH) groups in its molecular structure. This abundance of hydroxyl groups renders rayon more susceptible to oxidation reactions **[9]**. Notably, graphite felts face challenges due to their low kinetics in vanadium ion redox processes, as well as inadequate wettability in aqueous solutions, stemming from their inherent hydrophobic nature. These limitations hinder their widespread application in VFBs. Despite

the good electrocatalytic activity exhibited by carbon-based electrodes, their limited electrochemical reversibility of electrode toward the vanadium redox reactions necessitates the development of alternative modification methods. To enhance the electrochemical activity of carbon materials, various surface modification techniques have been explored, including nitrogenization, thermal, chemical, and plasma treatment. The purpose of these treatment methods is, mainly, enhancing the surface wettability and electrochemical redox activity **[7]**.

1.3. Thermal treatment modifications of VFB's electrodes

The electrocatalytic performance of carbon electrode materials can be significantly enhanced through oxidation treatment, which introduces surface oxygen functional groups to the surface. Among the various oxidation methods, thermal treatment has been recognized as an effective approach for the large-scale industrial production. This treatment method increases the presence of oxygen-containing functional groups, including C–OH, C=O, and C–OOH, leading to improved hydrophilicity as they act as catalytic sites for vanadium electrochemical redox reactions **[10].**

Figure 3 illustrates the possible mechanism for the vanadium redox reactions (both negative and positive) to understand the carbon-oxygen functional groups' catalytic role. During the charging process, ion exchange takes place as VO^{2+} species replace the H^+ ions associated with the C–OH functional groups. Subsequently, VO^{2+} ions are converted to VO_2^+ by gaining oxygen atom from the C–OH surface groups, which facilitates electron transfer along with the C–O–V bond. On the other hand, the discharge process involves the reverse redox reaction that occurs on the surface of the graphite felt electrodes. As shown in **Figure 3(b)**, this involves (1) the diffusion of V(III) ions from the bulk solution to the surface (2) the ion exchange with H^+ ions (3) the electron transfer between the electrode function groups (C–OH) and V(III), forming V(II) ions. Overall, the thermal treatment method enhances cell performance catalytically by generating oxygen-containing functional groups, improving wettability, and the surface area of the electrode material.

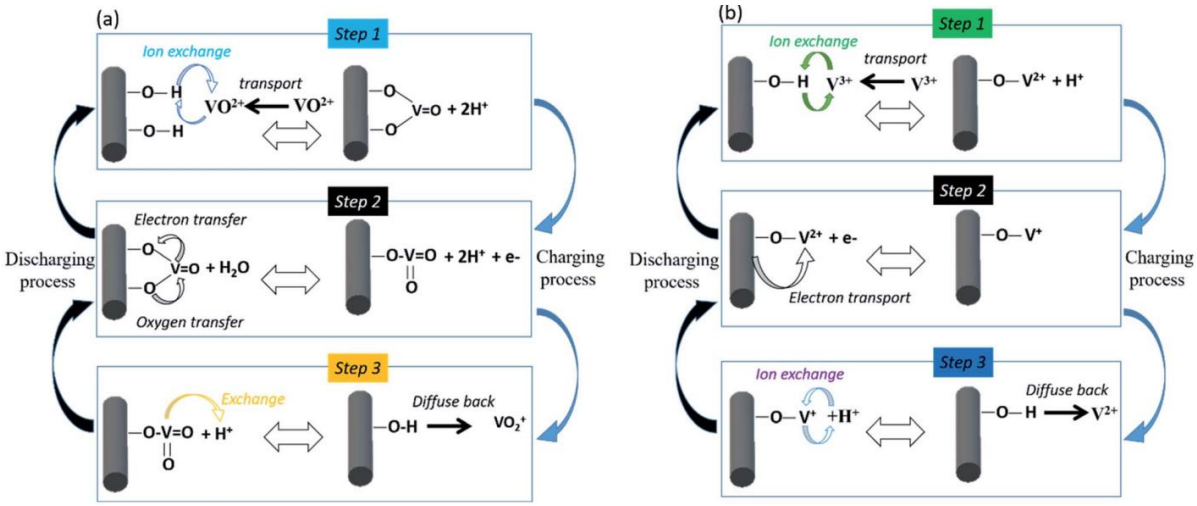

Figure 3: The proposed redox mechanism occurring on the surface of the thermally treated graphite felts for (a) the V(II)/V(III) redox couple within the anolyte and (b) V(IV)/V(V) couple within the catholyte of the VFB **[6].**

Although previous studies conducted thermal treatment of carbon felts **[4, 6, 10]**, the thermal treatment of graphite felts, particularly those made from rayon, for large-scale applications in VFBs has received limited exploration. A study conducted by Linder et al. focused on the thermal treatment of PAN **[16]**, but the investigation primarily concentrated on relatively prolonged treatment durations exceeding 8 hours, which are not suitable for practical industrial production. Hence, this research aims to present a cost-effective approach for the thermal treatment of two distinct types of graphite felts, PAN and rayon, to address the gap in knowledge regarding their industrial-scale applicability in VFBs. This work aims to investigate the effects of thermal treatment on the surface functionalization, surface area, and

wettability of the graphite felts used as electrodes in VFBs. It involves subjecting graphite felt electrodes to various temperatures and treatment times to enhance the surface activity of the electrode material for VFB by increasing the concentration of oxygen groups on the carbon surface. Through comprehensive electrochemical measurements, including cyclic voltammetry (CV), electrochemical impedance spectroscopy (EIS), and C/D tests, the effects of thermal treatment on the electrochemical activities and efficiency of VFBs are systematically analysed. By establishing a correlation between the thermal treatment parameters and the observed improvements in VFB efficiencies, this study aims to contribute to the development of more efficient and sustainable energy storage systems, facilitating the integration of renewable energy sources.

2. METHODOLOGY

2.1. Thermal treatment of graphite felts

In this study, two different types of graphite felt were utilized: rayon and PAN. These felts were commercially sourced from SGL Carbon Group in Meitingen, Germany, and their respective properties are presented in **Table 1**.

Table 1: Physical properties of graphite felt electrodes **[11]**.

	Carbon fibre precursor	Bulk density (g/cm^3)	Nominal thickness (mm)	Porosity (%)	BET surface area (m^2/g)	Electrical resistivity (Ω.mm)
GFD 4.6 EA	PAN	0.09	4.6	94	0.4	< 5
GFA 6 EA	Rayon	0.08	6.0	95	0.8	< 12

To perform the thermal treatment, the felts were placed in a furnace (PC L45/12, 1200 °C) and subjected to specific temperature conditions. For rayon, the temperatures range 300 to 500 °C, while the PAN ranged from 450 to 600 °C. The temperature gradually increased until the desired temperature was reached. Subsequently, the felt was kept cooling down for 2 hours to room temperature. The weight of the felts was measured before and after the treatment using a precise analytical laboratory scale (Kern ADJ 200-4) to analyse the weight loss as a function of time for each temperature.

2.2. Electrode preparation for the electrochemical measurements

The electrode preparation procedure for the electrochemical measurements is outlined in **Figure 4**. Initially, cylindrical graphite felt electrodes were obtained by punching them out from graphite felt sheets using hole punches. These electrodes were then cleaned with a stream of air to remove any potential contaminants. Next, the graphite felt pieces were centrally pierced by an isolated pencil mine (HB, 0.5 mm thickness). In this study, the use of a pencil mine as a working electrode was preferred over a platinum wire due to its non-reactive nature, thus avoiding the introduction of a reactive metal into the electrolyte solution. It was also determined that the pencil mine had a negligible impact on the signal generated by the felt electrodes, ensuring accurate electrochemical measurements **[8]**. It is important to note that graphite felts possess a porous structure that can trap air within their fibre matrix, potentially leading to inaccuracies in electrochemical measurements. To address this issue and ensure complete wetting of the felts with the electrolyte, the graphite felt electrodes were immersed in a 100 mL electrolyte solution and subjected to vacuum infiltration. This process effectively eliminates any trapped air and facilitates optimal penetration of the electrolyte within the graphite felts.

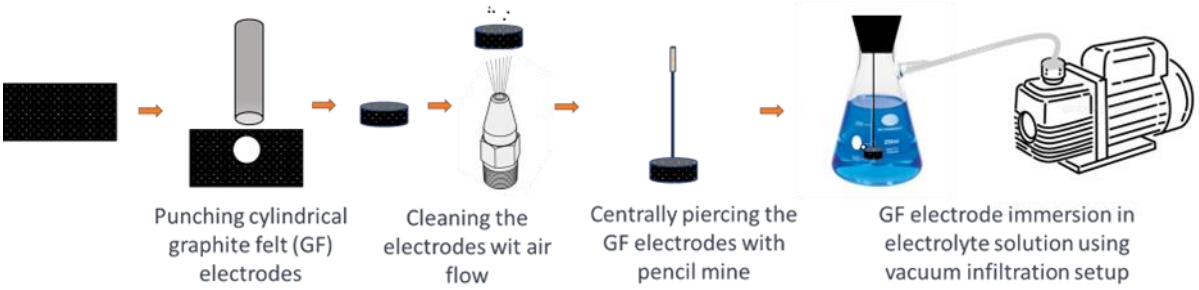

Figure 4: A scheme of the electrode preparation process for the electrochemical measurements.

2.3. Electrochemical measurements

To prepare for each measurement using cyclic voltammetry (CV), a pre-treatment procedure was conducted on the sample to ensure the best electrochemical cleaning. This involved subjecting the sample to specific potential ranges in both the positive and negative halves, using a scan rate of 100 mV/s for 50 cycles. The positive half-cell potential range was set from 0 to 0.5 V, while the negative half-cell spanned from 0 to -0.3 V *vs.* Ag/AgCl. For the subsequent electrochemical measurements, a three-electrode configuration was utilized. The working electrode (WE) was the graphite felt under investigation, the reference electrode (RE) was Ag/AgCl, and the counter electrode (CE) was a platinum grid. To ensure comparability, all three electrodes were positioned in a fixed manner within an electrochemical cell containing 20 mL of a 50 mmol/L electrolyte solution composed of $V^{2.5+}$ (equimolar ration of V(II): V(III) ions) and $V^{4.5+}$ (equimolar ration of V(IV):V(V) ions) ions for the negative and positive redox reactions, respectively, in a 1.0 mol/L H_2SO_4. CV measurements were performed within a scanning voltage window of 0.2 to 1.6 V and -0.05 V to -0.85 V *vs.* Ag/AgCl, for the positive and negative half cells, respectively, with a scan rate of 10 mV/s for 5 repetitive cycles.

Likewise, for the EIS experiments, the same three-electrode system configuration was used. The EIS measurements were conducted at open circuit voltage (OCV) (*vs.* Ag/AgCl reference electrode) over frequencies ranging from 0.01 to 20000 Hz with a perturbation amplitude voltage of 10 mV.

All the electrochemical measurements were carried out with a Gamry Interface 1010B potentiostat controlled by Gamry Framework software.

2.4. VFB single-cell assembly

To construct a VFB single-cell, two primary procedures were employed: the cell's main body assembly and the cell setup. The main body of the cell consists of various components, as depicted in **Figure 5**, and its assembly involves a series of sequential steps. First, the positive endplate was secured using screws and guide tubes. The positive distribution plate, copper current collector (CCC+) and bipolar plate (BPP+) were then stacked. The CCC and BPP play crucial roles in distributing the electrical current generated by the electrochemical reaction. Bipolar and membrane gaskets were then inserted to prevent electrolyte leaking. Next, the porous positive electrode and the ion-exchange membrane were placed. It should be noted that the more porous, active side of the positive electrode was positioned towards the membrane to maximize the electrolyte convection for the redox reaction. The dimensions of the electrode were precisely measured using a digital calliper, with an active area size of 5 cm^2 (20 x 25 mm) and a thickness of (4.7 $\pm$ 0.2) mm for the PAN and (5.5 $\pm$ 0.3) mm for the rayon. It is crucial for the flow frames, gaskets, and electrodes to have compatible thicknesses to achieve the desired compression rate for the whole cell (in the range of 24% to 27%). The electrode compression has an impact on the VFB cell resistance and overall performance; the resistance is decreasing by increasing the compression until reach constant values of resistance. According to the literature, the lowest values of resistances for the PAN and rayon graphite felts were achieved in the 24 to 27 % compression range **[15]**. Finally, the same components were assembled for the negative side of the cell in reverse order and the electrical connectors were added.

The second step was to setup up the small cell. Each of the two tanks was filled with 100 mL of a 1.6 mol/L vanadium electrolyte solution, and 10 mL of paraffin oil was introduced into the negative tank to prevent electrolyte oxidation caused by air exposure. Magnetic stirrers were placed in both tanks, and the pump was connected to the tanks. Finally, the assembled main body of the cell (depicted in **Figure 6)** was connected to each half-cell, creating a closed-loop system in which the electrolyte circulates between the two half-cells, as illustrated in **Figure 6.**

The C/D test was performed using the Battery Test System (NEWARE CT-4008T-5V6A) at two values of current densities (100 and 200 mA/cm^2). The upper voltage limit was 1.6 V for charging and the lower limit voltage was 1.0 V for discharging. In the initial charging process of a single VFB cell, a constant current density of 100 mA/cm^2 was applied, until reaching the upper limit of voltage of 1.6 V. Then, the discharging process started until the lower voltage limit (1.0 V). The same procedures were used for the 200 mA/cm^2 current density. This process of charge and discharge has been repeated for 10 cycles at each current density. The measurements were obtained from two assembled cells with graphite felts of similar dimensions and thickness. The two cells were subjected to the C/D test, and the efficiencies were calculated based on the average values obtained from these cells. Both cells comprised symmetric electrodes treated under identical thermal treatment conditions.

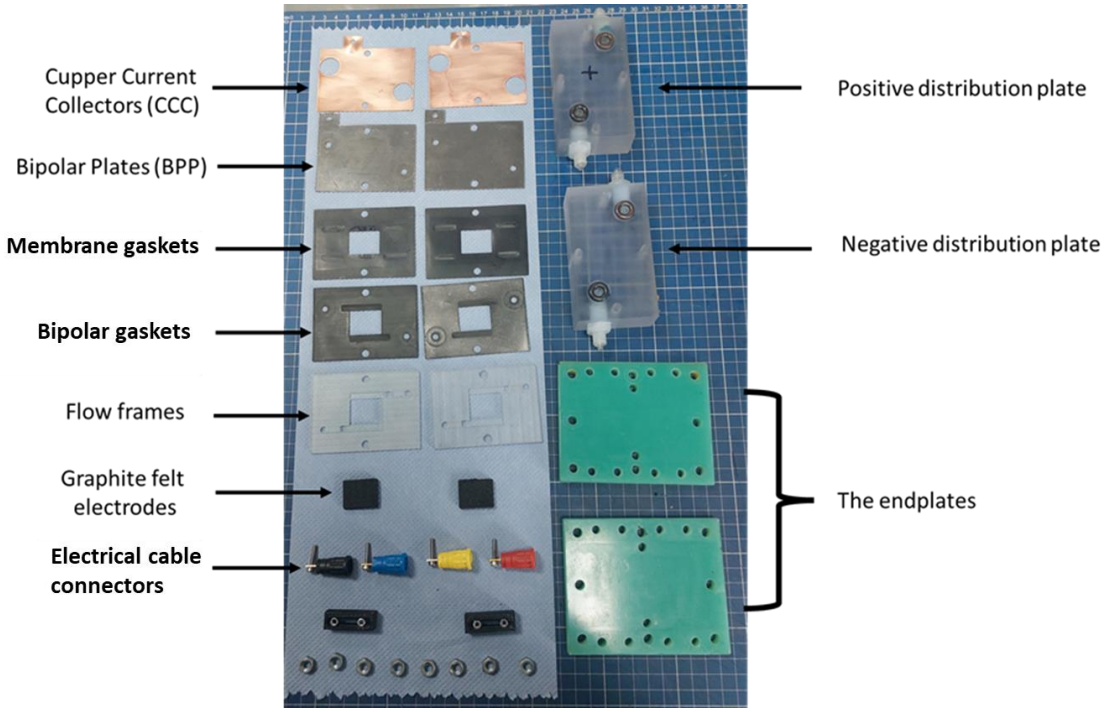

Figure 5: The components of the VFB small single cell.

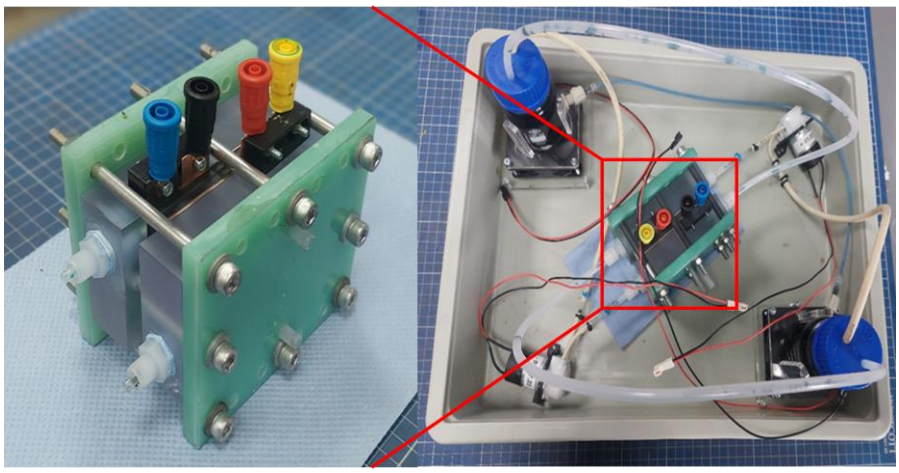

Figure 6: The VFB single cell main body (left) and full setup (right).

3. RESULTS AND DISCUSSION

3.1. Physicochemical properties of thermally treated of graphite felts.

Thermal treatment is a widely used and effective method in the industrial production of VFB. It results in the functionalisation of the graphite felt surface by introducing oxygen-containing functional groups. These groups increase the hydrophilicity of the surface and serve as active sites for vanadium redox processes. So, in this study, two commercially available graphite felts, rayon and PAN, were subjected to treatment at various temperatures for different durations. The key factors considered during the electrode treatments, such as the temperature and exposure time, were deliberately varied to investigate their effect on surface area, oxygen group formation and electrode wettability. By analysing the results, we delve into a comprehensive discussion regarding the treatment conditions of the process parameters that have a more pronounced influence on the physicochemical characteristics of the electrodes.

Dry samples of equivalent sizes from the graphite felts were subjected to temperatures ranging from 400 to 600 °C for PAN and from 300 to 500 °C for rayon. The selection of these temperature ranges was based on the thermal stability of the felts and preliminary thermogravimetric analysis (TGA) of untreated dry felt samples obtained from existing literature sources **[12, 17]**. Following the thermal treatment conducted at several temperatures, a noticeable change in the colour of the graphite felt can be visually observed. The impact of temperature on the colour of rayon graphite felt is depicted in **Figure 7**, where an increase in temperature corresponds to a darker coloration of the felt. Furthermore, when the temperature reached 500 °C, noticeable small pits emerged on the surface of the felt (identified by red circles), whereas at 600 °C, the felt exhibited almost full deterioration of the felts.

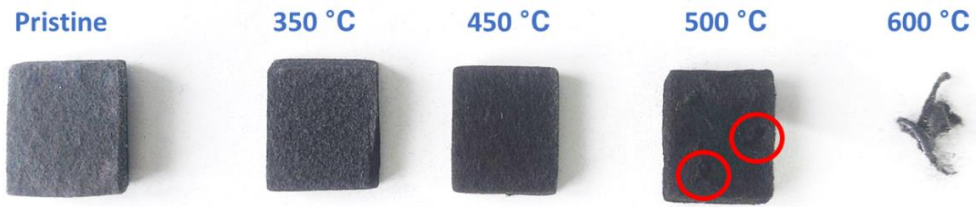

Figure 7: the effect of thermal treatment on the physical properties of the graphite felts.

Wight loss analysis was carried out on both rayon and PAN graphite felts at each temperature over 3 hours. PAN exhibits higher thermal stability in comparison to rayon, as evidenced by its ability to withstand higher treatment temperatures before experiencing degradation. The weight loss for the PAN at thermal treatment of 600 °C was less than 2% after 3 hours of treatment, which is consistent with previous literature, as Whitehead et al. reported a weight loss more than 1% in PAN only when exposed to temperatures above 500 °C for a duration of 2 hours **[12]**. On the other hand, although the weight loss recorded for the rayon below 400 °C was less than 1%, a significant increase in weight reduction was observed at higher temperatures, reaching 10% and 60% at 500 and 600 °C, respectively. Also, as shown in **Figure 8,** the weight loss of rayon after 3 hours of treatment was relatively low, about 2% and 4% at 400 and 450 °C, respectively. These results are consistent with the previously observed changes in the colour and morphology, indicating a consistent trend **[13].**

To investigate the effect of the thermal treatment on the wettability of graphite felts, distilled water droplets were applied to the felts surface. **Figure 9** shows the thermal treatment effect on the wettability, demonstrating that it increases upon the thermal treatment. In particular, the felts exposed to temperatures below 400 and 350 °C for the PAN and rayon, respectfully, showed negligible affinity for absorbing water droplets, while those treated at 500 and 400 °C absorbed the droplets within 30 seconds. In contrast, the felts treated at 600 °C for PAN and 550 °C for rayon showed an immediate absorption of the droplet position (shown as blue rectangle in **Figure 9 (b, c)**, indicating a high level of wettability. These results align with the results of Rabbow et al. **[13],** conducted on the PAN felts.

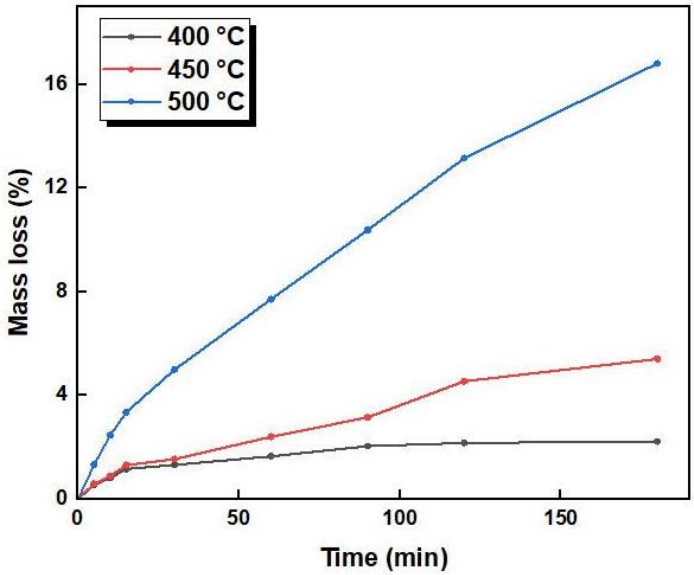

Figure 8: The effect of thermal treatment on the mass loss of rayon.

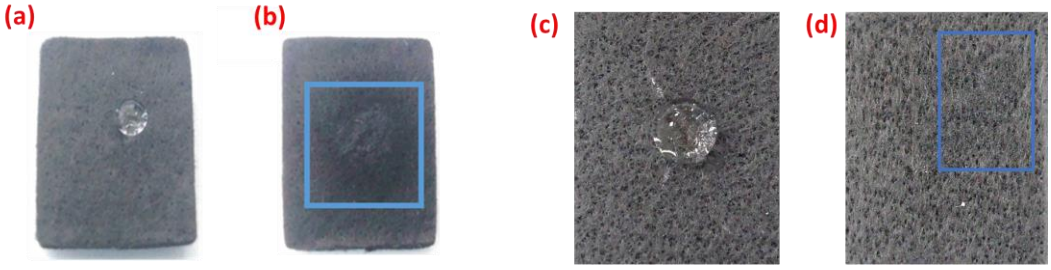

Figure 9: The impact of thermal treatment on the wettability for (a) rayon untreated, (b) rayon treated at 450 °C, (c) PAN untreated, and (d) PAN treated at 600 °C.

3.2. Electrochemical measurements

3.2.1. Cyclic Voltammetry

The basic principle of CV is to apply a voltage ramp to an electrochemical cell while measuring the resulting current response as a function of the applied voltage. The process involves a forward scan, a reverse scan, and a cyclic repetition. Cyclic voltammograms obtained from this CV technique have distinctive features containing valuable information about the studied electrochemical system. **Figure 10(a)** shows a typical cyclic voltammogram, including anodic (E_{pa}) and cathodic (E_{pc}) potential peaks, cathodic (I_{pc}) and anodic (I_{pa}) current peaks, and peak shapes**.** The shape and position of the peaks observed in cyclic voltammograms reveal essential details about the electrochemical processes occurring at the electrode-electrolyte interface. The peak current reflects the rate of electron transfer, while the peak potential indicates the thermodynamic feasibility of the redox reaction. In addition, the symmetry or asymmetry of the peaks can provide insight into the electrode kinetics and the reversibility of the redox reaction. Therefore, these quantitative measurements contribute to a deeper understanding of the system behaviour and allow comparisons between different experimental conditions.

In addition, CV can provide information on reaction mechanisms and distinguish between reversible, quasi-reversible, and irreversible redox reactions, as depicted in **Figure 10.** Reversible reactions exhibit equal peak currents in both forward and reverse scans, accompanied by an ideal Nernstian response in peak potentials, but irreversible reactions exhibit asymmetric peaks. A small potential difference (ΔE) between E_{pc} and E_{pa} indicates reversible redox reactions, whereas a larger ΔE indicates irreversibility or kinetically hindered processes. Furthermore, the peak current ratio of the oxidation peak current (I_{pa}) to the reduction peak current (I_{pc}) can be used to study the kinetics of the

electrochemical reactions. In the case of reversible reactions, this ratio should ideally approach 1, indicating equal magnitudes of the forward and reverse reactions. Consequently, CV facilitates comparative studies of the electrochemical performance between untreated and thermally treated electrodes. Critical features of the cyclic voltammogram undergo changes by changing the thermal treatment conditions. Parameters, such as peak currents, potential separations, and peak shapes, can be analyzed to assess Improvements in redox behaviour, kinetics, and stability.

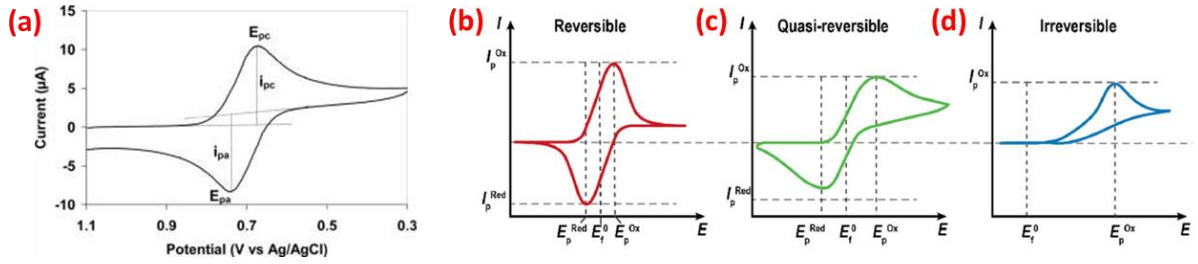

Figure 10: (a) The typical cyclic voltammogram for redox reactions, CV plots for (b) reversible (c) Quasi-reversible, and (c) Irreversible redox reactions **[8].**

First, several baseline experiments were performed to establish a reference point using the same acidic media (1 mol/L H_2SO_4) without the presence of vanadium ions. These baselines make it possible to distinguish the electrochemical behaviour between the solvent and the specific electroactive species under investigation, as determined by the measured current response. **Figure 11** presents the cyclic voltammogram of rayon and PAN electrodes in both 0.05 mol/L of $V^{4.5+}$ and $V^{2.5+}$ electrolyte and 1 mol/L H_2SO_4, demonstrating the minimal effect of the solvent on the observed current response. Subtraction of the baseline response from the overall CV signal enables accurate analysis of the electrochemical performance of the graphite felt electrode toward the redox-active vanadium species. Regarding the negative couple in 1 mol/L H2SO4, **Figure 11(c, d),** the observed sharp cathodic current at potentials below -0.2V *vs.* Ag/AgCl can be attributed to the hydrogen evolution reaction (HER). At these potentials, protons (H^+) from the sulfuric acid solution are reduced on the electrode surface, resulting in the evolution of hydrogen gas (H_2) **[20].**

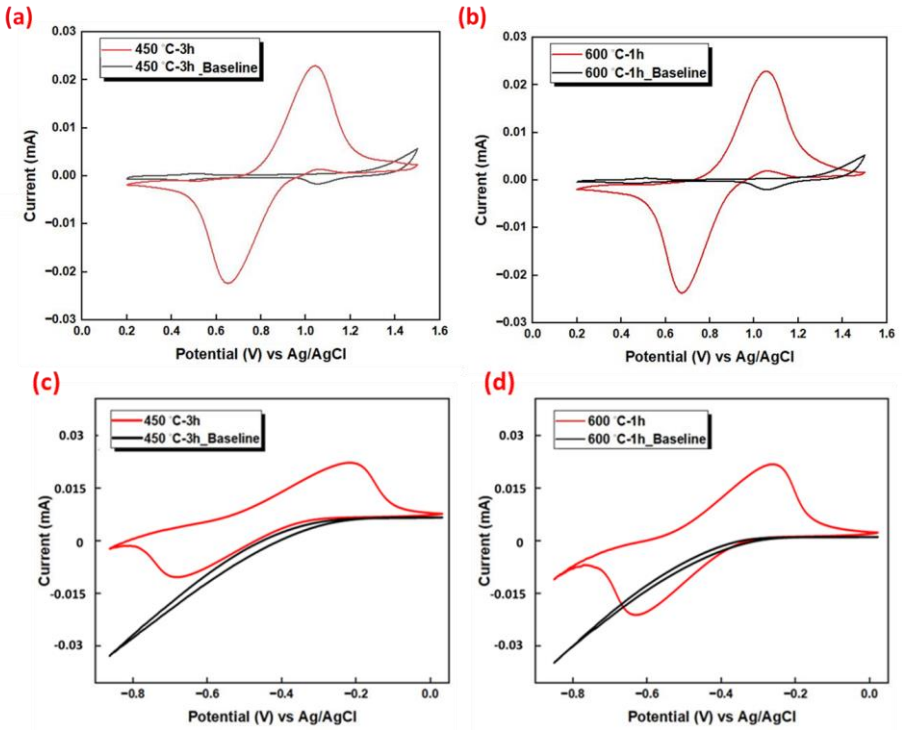

Figure 11: CV plots for (a) rayon treated at 450 °C-3h, (b) PAN treated at 600 °C-1h in 0.05 mol/L $V^{4.5+}$ in 1 mol/L H_2SO_4, and 1 mol/ L H_2SO_4 (the baseline) in potential window of 0.2-1.5 V *vs.* Ag/AgCl, (c) rayon 450 °C-3h, (d) PAN 600 °C-1h in 0.05 mol/L $V^{2.5+}$ in 1 mol/L H_2SO_4, and the baseline in a window of -0.85 to -0.05 V *vs.* Ag/AgCl.

Since this study aims to investigate the influence of varying temperatures and duration of thermal treatments on the electrochemical performance of two different graphite felts (rayon and PAN), CV is used to evaluate the electrochemical performance and reversibility for each half-reaction separately. The CV curves of different electrodes are shown in **Figure 12** and **Figure 13**, representing the redox couple reactions of the PAN and rayon, showing the variations in temperature and treatment time. The data obtained from the cyclic voltammograms are also summarized in **Tables 2** and **3**.

- **Positive half-reaction**

The characterization of the felts concerning the positive electrode reaction was carried out by CV in a 0.05 mol/L $V^{4.5+}$ solution with a 1 mol/L H_2SO_4 supporting electrolyte at 10 mV/s scan rate. For the positive electrode reaction, it is observed that an anodic peak between 1.1-1.2 V, corresponding to the oxidation of V(IV) to V(V), and a cathodic peak between 0.5-0.7 V, associated with reduction, occurred. **Figure 12(a)** shows an irreversible redox reaction for untreated PAN, as evidenced by the asymmetric peak shapes, where the anodic current peak was more pronounced than the cathodic peak. Similarly, for the untreated rayon shown in **Figure 12(b)**, the substantial peak potential separation (ΔE_p: 1.02 V) and the current density ratio ($i_a/i_c = 2.22$) indicated the electrochemical irreversibility of the V(IV)/V(V) redox couple. These observations suggest that the untreated felts aren't efficient in the reduction compared to the oxidation because the anodic peak (corresponding to the oxidation process) is higher than the cathodic one. Therefore, it reflects the presence of a considerable energy barrier between the oxidation and reduction processes for the untreated felts. This energy barrier hinders the efficient conversion of oxidized species, leading to a discrepancy in the current peak intensity.

In addition, the thermally treated electrodes exhibited improved electrochemical performance compared to the untreated electrode, as evidenced by the increased reversibility of the electrochemical redox reactions. For instance, as shown in **Figure 12(a)** and **Table 2**, increasing the treatment temperature of the PAN from 400 to 600 °C resulted in a decrease in the peak potential separation (0.76, 0.6, and 0.38 V for the 400, 500, and 600 °C treatment conditions, respectively) and a decrease in the anodic/ cathodic current ratio because the cathodic peak becomes more pronounced after the thermal treatment. Moreover, prolonging the treatment time at 600 °C further improved the electrochemical performance, achieving the optimal performance after 1 hour. The oxidation anodic current peak (i_a = 22.91 mA) and reduction current cathodic peak (i_c = 23.69 mA) were higher than those of the untreated electrodes (21.69 mA and 8.05 mA) and the treated electrodes at lower temperatures. The enhanced activity and reversibility of the treated PAN electrode can be attributed to the increased wettability induced by the thermal treatment in air and the resulting surface area.

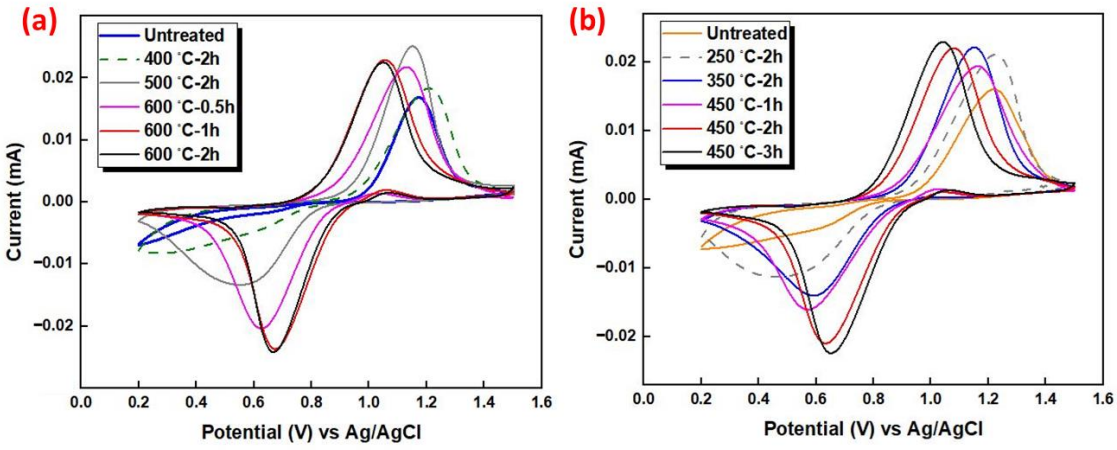

Figure 12: CV curves for (a) PAN, and (b) rayon electrodes in a solution of 0.05 mol/L $V^{4.5+}$ + 1 mol/L H_2SO_4 (the positive electrolyte) with a scan rate of 10 mV/s and potential of 0.2-1.5 V *vs.* Ag/AgCl (the positive potential window).

Similarly, in the case of rayon, **Figure 12(b)** demonstrates that thermal treatment of the felt significantly enhanced the reaction kinetics, with ΔE_p decreasing to 0.76 V for the felt treated at 250 °C compared to 1.02 V for the untreated rayon. **Table 2** indicates that the most significant improvement

in electrochemical reversibility was observed after treating the felts at 450 °C for 3 hours, with the lowest ΔE_p value within the series (0.39 V) and the I_a/I_c value closest to 1 (1.03). Therefore, the enhancement in electrode performance appears to be strongly related to the increased electrode-electrolyte interface and the presence of functional groups on the surface of the graphite fibre. It is worth noting that the electrochemical performance of the graphite felts deteriorated when treated at temperatures above 450 °C, most likely due to felt degradation, as indicated by its high weight loss.

- **Negative half-reaction**

On the other side, the characterization of the felts concerning the negative half reaction was conducted in a 0.05 mol/L $V^{2.5+}$ in 1 mol/L H_2SO_4 at the same scan rate of 10 mV/s. The cyclic voltammograms in **Figure 13** demonstrate that the negative redox reactions for the untreated graphite felts (PAN and rayon) are highly irreversible, as evidenced by the pronounced degree of asymmetry. It is also observed that the cathodic peaks are poorly developed, and both peak currents are significantly reduced for the untreated graphite felts. This observed unfavourable behaviour can be attributed to the irreversible and competitive hydrogen evolution, as it occurs within the same potential range as the V(II)/V(III) reduction (below -0.2 V *vs.* Ag/AgCl). The pronounced hydrogen evolution explains the slight increase in cathodic peak currents and the asymmetric shape. Extensive hydrogen gas bubble formation was observed during the CV measurements when untreated graphite felts (PAN and rayon) were used as the negative electrode, unlike the treated felts, confirming the previously mentioned hypothesis. The presence of hydrogen gas generated at the negative electrode reduces the charge transfer efficiency and blocks reaction sites within the electrode.

For example, when considering PAN, the CV plots shown in **Figure 13(a)** provide compelling evidence of significant differences between the studied felts. This is further illustrated by the data in **Table 2** and **3**, which show that thermally treated graphite felts exhibit significantly improved electrochemical performance in the V(II)/V(III) redox processes. This is evident from the voltammograms, like an ideal system, with higher anodic and cathodic peak currents and narrower potential separation values. However, it should be noted that the cathodic and anodic peaks still lack significant symmetry for the 400 and 500 °C treatment conditions. In addition, the electrochemical properties of the felts are improved when treated at 600 °C compared to the untreated graphite felts due to the increase in their oxygen content, which leads to enhanced wettability. Specifically, as shown in **Table 2**, after treatment at 600 °C for 0.5 hours and 2 hours, the Ia/Ic values are recorded as (0.89, 0.93), and the ΔE_p values are (0.33, 0.36 V), respectively. However, the most favourable I_a/I_c ratio (0.93) and the narrowest potential separation (0.33 V) are observed after 1 hour of treatment at 600 °C, confirming the positive results of the redox reaction.

Similarly, in the case of rayon, the performance of samples treated at 250 °C shows minimal improvement compared to the untreated samples. **Table 3** shows that increasing the treatment temperature enhances reversibility. The I_a/I_c ratio increases to 0.91 after 2 hours of treatment at 450 °C, compared to 0.62 and 0.61 for 250 °C and 350 °C, respectively. Furthermore, the highest reversibility is observed for rayon felts treated at 450 °C for 3 hours, with an I_a/I_c value of 0.93 (closest to 1) and ΔE_p of 0.41 (lowest). Therefore, the optimum treatment conditions for rayon graphite felts (rayon) in both positive and negative half-reactions are at 450 °C for 3 hours.

The results from the negative half-reaction align with those obtained from the positive side, reflecting that the thermal treatment improves the kinetics of the electrochemical negative reaction for both felts. **Figure 13** clearly demonstrates that the treatment reduces the occurrence of the hydrogen evolution reaction compared to the V(II)/V(III) redox reactions. This is evident from the pronounced cathodic and anodic peaks observed after treatment. Overall, the observed improvements in electrochemical activity for both half-reactions after the thermal treatment can be attributed to reducing the overpotential for the redox flow batteries, thereby improving their overall performance.

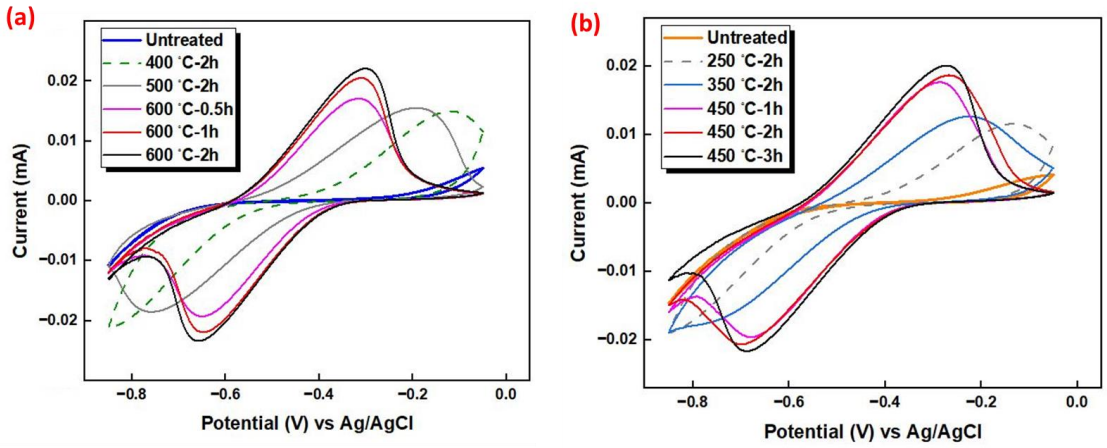

Figure 13: CV plots for (a) PAN, and (b) rayon electrodes in a solution of 0.05 mol/L $V^{2.5+}$ in 1 mol/L H_2SO_4 (the negative electrolyte) at 10 mV/s and potential of -0.85 V to -0.05 V *vs.* Ag/AgCl (the negative potential window).

Table 2: Electrochemical insights of the PAN graphite felt electrodes recorded from the cyclic voltammograms.

	Positive Half Reaction						Negative Half Reaction					
Temperature	**E_a (V)**	**I_a (mA)**	**E_c (V)**	**I_c (mA)**	**I_a/I_c**	**E_a-E_c (V)**	**E_a (V)**	**I_a (mA)**	**E_c (V)**	**I_c (mA)**	**I_a/I_c**	**E_a-E_c (V)**
Untreated	1.18	21.69	0.21	8.05	2.7	0.97	-0.05	5.52	-0.85	10.81	0.51	0.8
400 °C-2h	1.16	24.4	0.4	9.69	2.52	0.76	-0.12	15	-0.85	21.23	0.71	0.73
500 °C-2h	1.15	24.98	0.55	13.23	1.89	0.6	-0.21	17.03	-0.75	20.72	0.82	0.54
600 °C-0.5h	1.13	21.78	0.63	20.39	1.07	0.50	-0.32	17.12	-0.65	19.26	0.89	0.33
600 °C-1h	1.06	22.91	0.67	23.69	0.97	0.38	-0.31	20.56	-0.64	21.94	0.93	0.33
600 °C-2h	1.05	22.53	0.67	24.19	0.93	0.38	-0.30	22.12	-0.66	23.38	0.93	0.36

Table 3: Electrochemical insights of the rayon graphite felt electrodes recorded from the cyclic voltammograms.

	Positive Half Reaction						Negative Half Reaction					
Temperature	**E_a (V)**	**I_a (mA)**	**E_c (V)**	**I_c (mA)**	**I_a/I_c**	**E_a-E_c (V)**	**E_a (V)**	**I_a (mA)**	**E_c (V)**	**I_c (mA)**	**I_a/I_c**	**E_a-E_c (V)**
Untreated	1.22	16.06	0.20	7.22	2.22	1.02	-0.05	4.13	-0.85	14.61	0.28	0.8
250 °C-2h	1.22	21.13	0.47	11.29	1.87	0.76	-0.13	11.61	-0.85	18.95	0.61	0.72
350 °C-2h	1.15	22.16	0.59	14	1.58	0.56	-0.22	12.67	-0.72	20.31	0.62	0.49
450 °C-1h	1.16	19.42	0.57	16.02	1.21	0.59	-0.25	18.1	-0.68	20.97	0.86	0.43
450 °C-2h	1.08	22.04	0.63	20.97	1.05	0.45	-0.27	18.7	-0.70	20.63	0.91	0.43
450 °C-3h	1.04	22.96	0.65	22.39	1.03	0.39	-0.27	20.11	-0.69	21.62	0.93	0.41

3.2.2. Scan rate effect on the electrochemical performance

In order to gain deep insight into the kinetics of the electrochemical redox reaction, CV measurements were performed at different scan rates for the V(IV)/V(V) redox couple. **Figure 14** and **Figure 15** show these curves for the PAN and rayon electrodes, respectively. It is noted that the peak current (i_a/i_c) ratio remains relatively constant over all scan rates. This constancy can be attributed to the increased electron transfer that occurs on the electrode surfaces as the scan rate increases. Also, raising the scan rate leads to a downward shift of the reduction potential and an upward shift of the oxidation potential.

To understand the effect of thermal treatment on the mass transfer of the redox reactions involved, the anodic peak current was plotted against the square root of the scan rate, using the Randles-Sevcik

equation. The direct proportionality between the anodic peak current of V(IV)/V(V) and the square root of the scan rate implies that a diffusion process governs the redox behaviour of electroactive species at all electrodes. By evaluating the slopes of each electrode plot, the electrochemical surface area (ECSA) in square metres (m^2) can be derived. ECSA represents the surface area available for the electron transfer process at the electrode/electrolyte interface **[17]**. The determination of ECSA for the V(IV)/V(V) redox system can be achieved by using the Randles-Sevcik equation as follows:

$$\mathbf{i_p = 2.69 \times 10^5\ A\ n^{\frac{3}{2}}\ C_0\ \sqrt{v\ D}}$$

Where i_p (in A) is the peak current of the oxidation peaks from V(IV) to V(V), n is the number of electrons transferred in the redox reaction, A is the active ECSA (cm^2), C_0 is the bulk concentration of the electroactive species (mol/cm^3), v is the scan rate (V/s), and D is the diffusion coefficient of the electroactive species (cm^2/s). Therefore, the ECSA can be expressed from the slop of the i_p *vs* $v^{1/2}$ plot, in which higher values of slope reflect higher ECSA.

Figure 14 and **Figure 15** provide information on the effect of scan rate on the peak current of untreated PAN and rayon, respectively. They show an absence of a linear correlation between the current peak and the scan rate for both felts, confirming the irreversibility of the redox reaction in the untreated electrodes **[19].** However, after the thermal treatment of the graphite felts, distinct peaks are observed across all scan rates, and the peak current exhibits a linear relationship with the square root of the scan rate, which means that the reactions become reversible and are governed by mass transport mechanisms. In the case of PAN, the linearity begins to manifest itself at a treatment temperature of 500 °C, as evidenced by the corresponding R^2 values in **Table 4**, which shows the data obtained from the relationship between peak current and the square root of the scan rate.

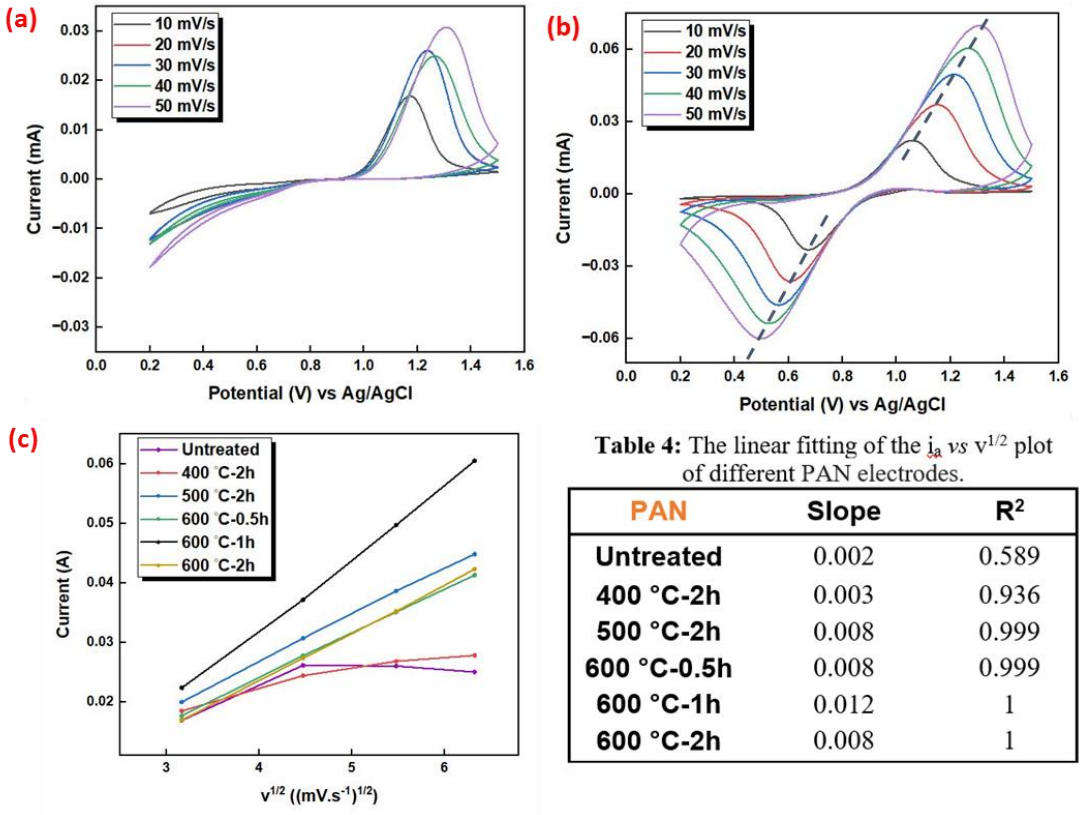

Table 4: The linear fitting of the i_a *vs* $v^{1/2}$ plot of different PAN electrodes.

PAN	Slope	R^2
Untreated	0.002	0.589
400 °C-2h	0.003	0.936
500 °C-2h	0.008	0.999
600 °C-0.5h	0.008	0.999
600 °C-1h	0.012	1
600 °C-2h	0.008	1

Figure 14: CV plots at various scan rates for PAN electrodes (a) untreated, (b) treated at 600 °C for 1h, and (c) the relationship between the anodic current peak versus the square root of scan rate for the positive redox couple.

Table 4 represents that the slopes are enhanced at 600 °C (0.0079 and 0.0121) compared to the untreated and 400 °C treated PAN (0.025, 0.003). The increase in the current means that there is an

increase in the ECSA, indicating a faster mass diffusion process on the porous electrode. Likewise, the rayon electrodes show a remarkable linear correlation between the peak current and the square root of the scan rates ($v^{1/2}$) (depicted in **Figure 15**). By examining the slope of each electrode (**Table 5**), the ECSA was determined in the following order: rayon treated at 450 °C > 250 °C > untreated samples. Intriguingly, the slope remains almost constant for all electrodes treated at 450 °C, regardless of the duration of treatment. However, CV and EIS measurements show that the electrochemical performance peaks after 3 hours of treatment, suggesting that this treatment condition is optimal for rayon electrodes.

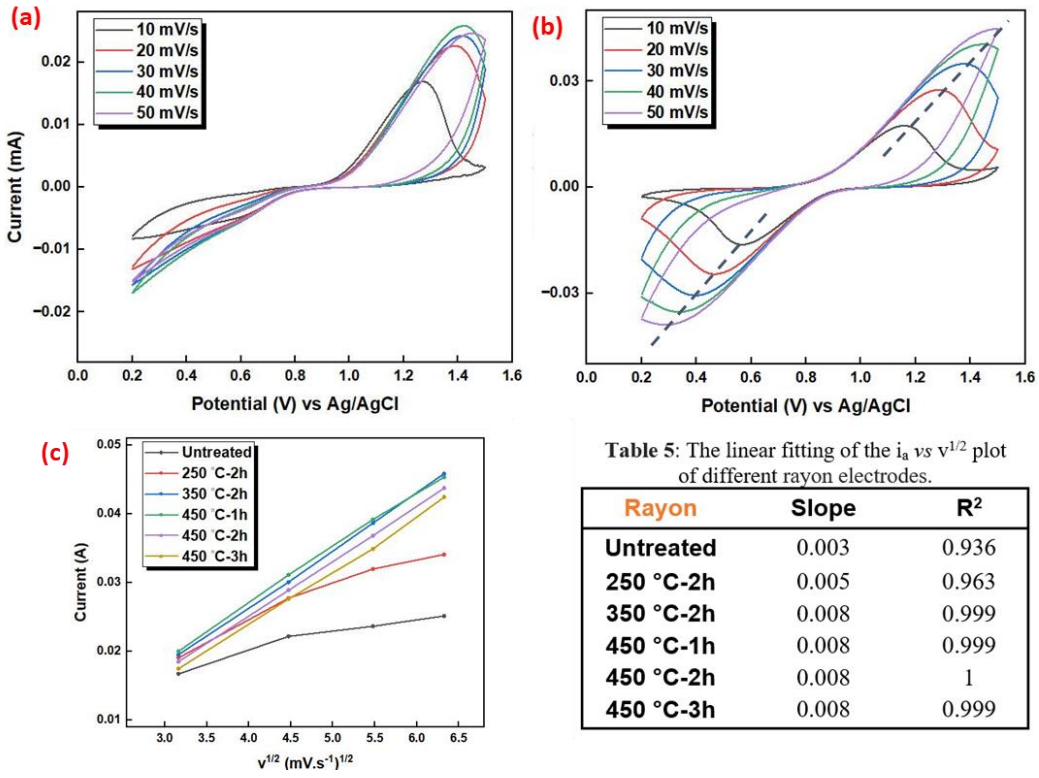

Table 5: The linear fitting of the i_a *vs* $v^{1/2}$ plot of different rayon electrodes.

Rayon	Slope	R^2
Untreated	0.003	0.936
250 °C-2h	0.005	0.963
350 °C-2h	0.008	0.999
450 °C-1h	0.008	0.999
450 °C-2h	0.008	1
450 °C-3h	0.008	0.999

Figure 15: CV plots at various scan rates for PAN electrodes (a) untreated, (b) treated at 600 °C for 1h, and (c) the relationship between the anodic current peak versus the square root of scan rate for the positive redox couple.

3.2.3. Electrochemical Impedance Spectroscopy

Electrochemical impedance spectroscopy (EIS) is a technique that provides researchers with valuable insight into the behaviour of electrochemical systems. In principle, the conventional approach to EIS involves studying the response of a system to a sinusoidal perturbation applied voltage ($\mathbf{V(t) = V_0 e^{-i\omega t-\varphi v}}$) and measuring the subsequent current response ($\mathbf{I(t) = I_0 e^{-i\omega t-\varphi i}}$). Here, ω is the angular frequency, V_0 and I_0 are the amplitudes of the oscillating signals, and φ symbolizes the phase of the complex voltage and current. In accordance with Ohm's law, impedance (Z) can be calculated as the ratio of voltage to current (V(t)/I(t)), yielding the expression:

$$\mathbf{Z = \frac{V(t)}{I(t)} = \frac{V_0}{I_0}\frac{e^{-i\omega t-\varphi v}}{e^{-i\omega t-\varphi i}} = Z_0 e^{i\theta} = Z' + iZ''}$$

Here, θ characterizes the phase shift between the voltage and current, while Z' and Z" correspond to the real and imaginary components of the impedance, respectively. By varying the frequency of the applied signal, EIS can probe different processes occurring at the electrode-electrolyte interface.

One of the most effective approaches to interpret EIS data is the use of equivalent circuits. For systems involving a redox pair, a widely recognized equivalent circuit, known as the Randles' equivalent circuit,

is commonly used (depicted in **Figure 16(b)**). This circuit includes various elements like the solution resistance (R_s), which represents the bulk properties of the electrolyte; the Warburg impedance (Z_W), representing the mass transport diffusion; the double-layer capacitance (C_{dl}); and the charge-transfer resistance (R_{CT}), which reflect the surface properties of the electrode-solution interface. For visual representation of EIS data, the corresponding Nyquist plot (**Figure 16(a)**), which displays the real and imaginary components of the impedance, is often represented using a Randles circuit.

The Nyquist plot, with its semicircular shape, provides crucial insight into the electrochemical system. A smaller diameter of the semi-circle indicates a faster charge-transfer process, while a larger diameter suggests a slower reaction. The intersection of the semi-circle with the real axis (Z') at low frequency represents the solution resistance, R_s, while the intersect at high frequency corresponds to $R_s + R_{CT}$, which provide important information about the kinetics of the electrochemical reaction. Additionally, deviations from the ideal semicircular shape can indicate phenomena such as adsorption, double-layer capacitance, and heterogeneous charge-transfer. By analysing the deviations and fitting mathematical models to the Nyquist plot, researchers can extract quantitative information about the various electrochemical processes occurring within the system.

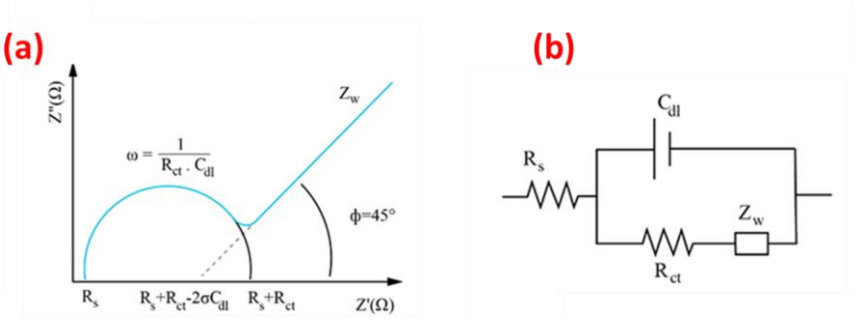

Figure 16: (a) Typical Nyquist plot obtained from the EIS measurements of a redox couple, and (b) the corresponding equivalent circuit of the redox couple **[18]**.

To effectively analyse and interpret the Nyquist plots obtained from our EIS measurements, they have been fitted with an equivalent circuit as depicted in **Figure 17**. The circuit components are defined as follows: R_s represents the solution resistance; CPE_1 and R_c represent the capacitance and resistance associated with the interaction between the graphite felt fibres and the electrolyte. CPE_2 and R_{CT} represent the electric double-layer capacitance and the charge-transfer resistance at the interface between the electrode and the electrolyte solution, while CPE_3 is the diffusion capacitance associated with the diffusion process of vanadium ions. It is worth noting that due to the uneven distribution of potential within the porous felt electrode, flattening of the semi-circle is observed. Consequently, in the equivalent circuit, constant phase elements (CPE_2 and CPE_3) were used in the equivalent circuit instead of ideal capacitors to accurately reflect the non-ideal behaviour of the electrode-electrolyte double layer and the diffusion capacitances. Within the equivalent circuit, CPE_3 corresponds to the diffusion process of vanadium ions, which can be described by the expression: $\mathbf{CPE_3 = Y^{-1}(j\omega)^{-n}}$, where Y is the pre-factor and n is the exponent of CPE_3, respectively. It should be noted that an increase in the pre-factor Y implies a decrease in the impedance associated with diffusion.

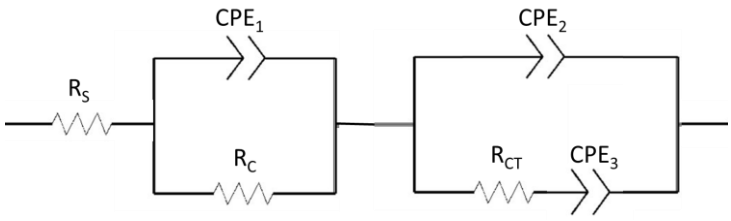

Figure 17: The equivalent circuit of EIS measurements of vanadium redox reactions in anolyte and catholyte.

The obtained Nyquist plots in **Figure 18** and **Figure 19** exhibit distinct characteristics, consisting of a semi-circle at high frequencies and a linear part at low frequency range. This observation indicates that both redox reactions undergo a combination of electron transfer and mass transfer processes, known as mixed control. The semi-circle observed in the high frequency range corresponds to the electron transfer step, with its radius representing the charge-transfer resistance (R_{CT}) between the electroactive species of the electrolyte and the active sites on the electrode surface. A smaller radius corresponds to lower values of the charge-transfer resistance, implying a faster electron transfer reaction. The linear part observed at low frequencies range shows the diffusion processes taking place within the graphite felt electrode (mass transfer step).

The data obtained from the EIS plots indicated that the Rs values of all the graphite delt electrodes were almost identical (around 4.5 Ω) for both negative and positive half-reactions. This suggests that the measurements for each half reaction were accurately carried out under identical conditions, like the electrolyte volume and concentration. However, for the positive redox couple, the charge-transfer resistances (R_{CT}) of the PAN exhibit significant variation, depending on the temperature and duration of the treatment. As shown in **Table 6**, R_{CT} value of the untreated sample (440 Ω) decreases with increasing temperatures to 153, 43.6, and 4.88 Ω at 400, 500, and 600 °C, respectively, indicating an enhancement in electron transfer kinetics. The PAN electrode treated at 600 °C for 1 hour exhibited the lowest charge-transfer resistance (3.23 Ω), indicating the fastest electron transfer rate. This finding further supports its superior electrochemical performance in facilitating the oxidation of V(IV) to V(V) and vice versa in the positive redox couple. In addition, the PAN electrode shows that after thermal treatment, there is an increase in Y, which is the pre-factor of the CPE_3 that describes the diffusion capacitance. Such increase indicates enhancements in the diffusion capacity of ions within the pores of the graphite felts compared to the untreated PAN. The findings of the negative half reaction (illustrated in **Figure 19** and **Table 6**) are in agreement with those obtained from the positive side, demonstrating the consistency of the results. These improvements can be attributed to the functionalization of the electrode surface with oxygen-containing functional groups, which act as active sites, facilitating the V(IV)/V(V) redox reaction.

There are significant differences between the untreated rayon electrodes and those subjected to thermal treatment. In the positive electrolyte (**Figure 18**), the R_{CT} value of the untreated rayon reaches around 128 Ω, which is 8 times higher than the value for the electrodes treated for 2 hours at 350 °C (16.4 Ω), indicating a lower electrochemical activity of the untreated electrodes. However, the thermal treatment significantly reduces the R_{CT}, with the lowest value observed in the felt treated at 450 °C (2.1 Ω). This result suggests a faster electron transfer process of the vanadium-ion redox reaction occurring with the treated electrodes. Moreover, the treated samples exhibit larger Y values for both oxidation and reduction processes compared to the untreated samples, indicating improved mass transport rate. Considering the charge-transfer resistances of the rayon electrodes towards V(II)/V(III), the negative redox couple, the descending order is as follows: untreated rayon > rayon-250 °C > rayon-350 °C > rayon-450 °C. In comparison, the R_{CT} values of the rayon electrodes treated at 450 °C for 3 hours are significantly the lowest (1.3 Ω), suggesting a significant increase in the electrochemical activity of these electrodes due to the thermal treatment.

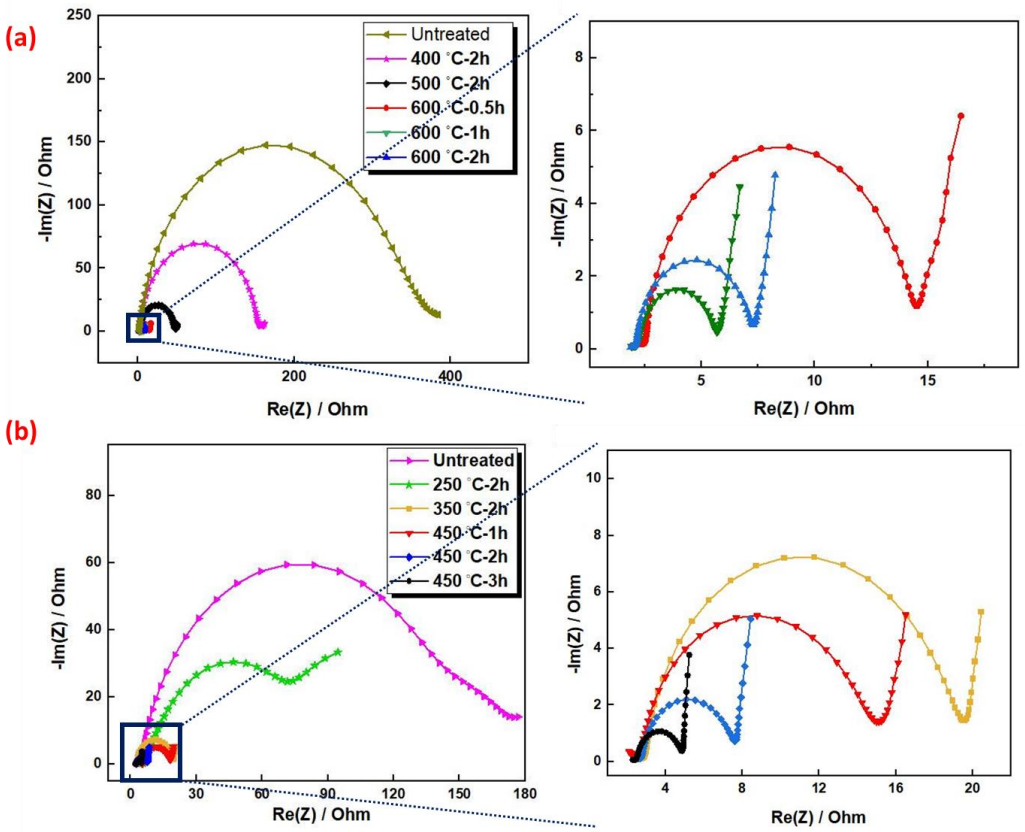

Figure 18: EIS plots showing the effect of thermal treatment on the electrochemical activity for (a) PAN, and (b) rayon electrodes in the positive electrolyte at OCV in the frequency range of 20000 to 0.01 Hz.

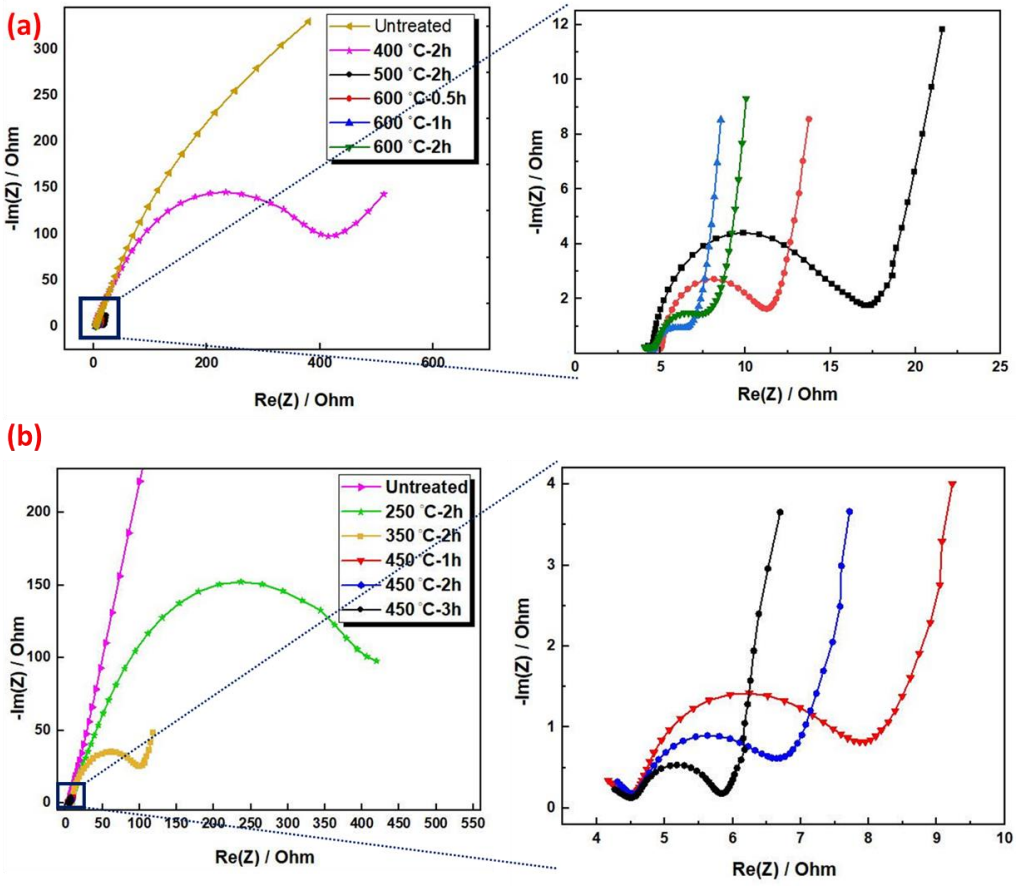

Figure 19: EIS plots showing the effect of thermal treatment on the electrochemical activity for (a) PAN, and (b) rayon electrodes in the positive electrolyte at OCV in the frequency range of 20000 to 0.01 Hz.

Table 6: Fit parameters obtained from the equivalent circuit model in Figure 17 for EIS Nyquist plots of treated electrodes (PAN and rayon) within both redox couples.

	Positive Half Reaction			Negative Half Reaction				Positive Half Reaction			Negative Half Reaction		
PAN	R_{CT}	CPE_3		R_{CT}	CPE_3		**Rayon**	R_{CT}	CPE_3		R_{CT}	CPE_3	
		Y	n		Y	n			Y	n		Y	n
Untreated	440	0.002	0.85	--	--	--	**Untreated**	128	0.01	0.94	--	--	--
400 °C-2h	153	0.01	0.95	511	0.005	0.91	**250 °C-2h**	51.08	0.001	0.85	485.4	0.005	0.89
500 °C-2h	43.6	1.39	1.3	12.4	0.20	0.82	**350 °C-2h**	16.37	2.3	0.83	94.39	0.06	0.63
600 °C-0.5h	12.2	1.83	0.81	6.76	0.29	0.85	**450 °C-1h**	12.1	1.89	0.77	3.49	0.61	0.82
600 °C-1h	3.23	3.06	0.86	1.47	0.36	0.94	**450 °C-2h**	4.82	2.81	0.89	2.58	0.72	0.88
600 °C-2h	4.88	2.69	0.87	4.08	0.25	0.91	**450 °C-3h**	2.11	4.85	0.97	1.3	2.42	0.87

3.3. VFB single-cell performance

Charge-discharge tests were conducted on the graphite felt electrodes to evaluate their performance within a single-cell of VFB. Generally, three types of efficiencies can be employed to analyze the VFB performance, which are coulombic efficiency (CE), voltage efficiency (VE), and energy efficiency (EE). Coulombic efficiency is the charge efficiency, resulting from transferring the electrons within the VFB. It is expressed as the ratio of total charge obtained from the VFB to the input charges. This efficiency describes the energy losses due to side reactions, electrode polarization, and crossover of vanadium ions through the ion-selective membrane **[21]**. Higher coulombic efficiency is desirable as it indicates minimal energy loss within the battery system. Voltage efficiency refers to the ratio of the average value of potential during the discharge process to the average value of potential during the charging process. It represents various losses, including the overpotential and electrolyte crossover. Energy efficiency measures the ratio of energy output during discharge to the energy input during the charging process. From its definition, it can be expressed by the product of the voltage and coulombic efficiency as follow (**EE = CE × VE**). Therefore, it considers the overall losses, including ohmic losses, voltage drops, and self-discharge **[22].** A higher energy efficiency indicates a more efficient VFB system, as it signifies more significant amount of stored energy, which is successfully utilized during discharge.

To validate the effectiveness of thermal treatment in improving the performance of VRBs, a C/D test was performed on a variety of electrode samples. **Figure 20(a)** illustrates the continuous C/D cycles of single-cell VFBs, encompassing 10 consecutive cycles at a lower current density of 100 mA/cm^2, followed by 10 cycles at a higher current density of 200 mA/cm^2. To avoid side reactions such as the evolution of O_2 and H_2, the operating voltage was maintained within the range of 1.0 to 1.6 V. It should be pointed out that one of the key factors to assess the superior capacity of the VRB is the high initial discharge value of voltage and low initial charge voltage.

As an example, **Figure 20(b)** displays the charge discharge voltage curve at a fixed current density of 100 mA/cm^2 for the untreated and treated PAN, within the voltage range of 1.0 V to 1.6 V. Apparently, the thermal treatment of the graphite felts elevates the discharge voltage plateau compared to the untreated PAN, which yielded a significant improvement in the capacity. Notably, the treaded PAN produced a higher discharge potential (1.45 V) and lower charge potential (1.3 V) compared to the untreaded PAN (1.2 and 1.5 V), reflecting a reduction in electrochemical polarization resistance for the thermally treated PAN. Moreover, due to the internal resistance of the VFB single cell, a significant decrease in cell potential is observed for the untreated PAN when the direction of current flow shifted

from charging to discharging, as evidenced by **Figure 20(b)**. However, the potential drop is much lower in the VFB, incorporating treated PAN electrodes, reflecting smaller internal resistance.

In **Figure 20(c)**, the voltage profiles during charging and discharging at a current density of 200 mA/cm^2 demonstrate comparable performance, in which the initial charging potential of the treated samples is lower; 1.43 V compared to 1.53 V for the untreated electrodes. It is crucial to note that an increase in current density results in a reduction in the charging potential caused by both ohmic and polarization resistance. Overall, the findings depicted in **Figure 20** indicate that the thermal treatment resulted in improved battery performance in terms of the voltage plateau during discharge and the duration of discharge. The data presented in **Table 7** and **Table 8** represent the average efficiencies observed over 10 consecutive cycles for each current density. The measurements were obtained from two assembled cells with graphite felts of similar dimensions and thickness. Throughout all the tests, the cell's geometry and membrane remained constant, so changes in energy efficiency corresponds to a change in electrode activity.

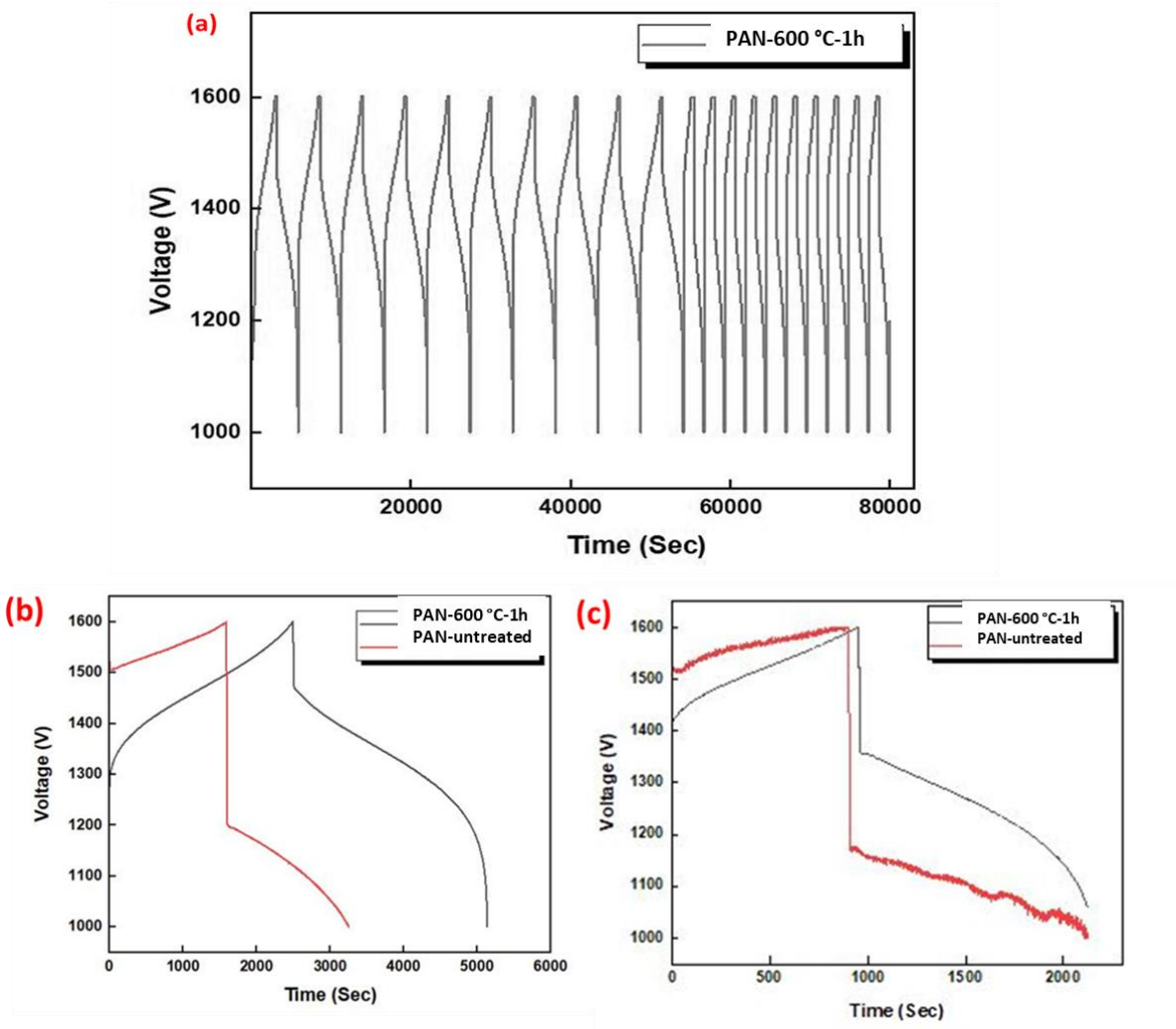

Figure 20: (a) The charge-discharge voltage profile of VFB single-cell employed different treated PAN for 10 cycles at each current density. A comparison of the two distinct symmetric VFB single cells at (b) 100 mA/cm^2 current density, and (c) 200 mA/cm^2 current density.

Table 7 shows the results of C/D experiments conducted on VFB, incorporating symmetric electrodes of untreated and thermally treated PAN. It is evident that treating the PAN for 1 hour at 600 °C resulted in a slight increase in the average CE compared to the untreated PAN (from 98.61 to 99.33%). This

enhancement can be attributed to the decreased duration of the C/D cycles, resulting in reduced vanadium ion crossover through the membrane. Furthermore, upon thermal treatment, the average VE values exhibited an increasing trend, rising from 69.6% for the untreated samples to 73.6%, 84.28%, and 88.1% for the samples treated at 400, 500, and 600 °C for 2 hours, respectively. The symmetric cell with PAN electrodes treated at 600 °C for 1 hour demonstrated the most outstanding performance, with a remarkable 19% VE increase compared to untreated PAN. Moreover, the EE, which is determined by multiplying CE and VE, followed the same pattern as the VE. Notably, the highest EE was observed after subjecting the electrodes to a 1-hour treatment at 600 °C, which is 1.3 times more than the VE of the untreated PAN.

Table 7 also shows that EE and VE decrease with increasing the current density to 200 mA/cm^2. This is because the fast charge or discharge rate leads to higher overpotential, resulting in reduced C/D capacity due to a narrower potential window. When operating at higher current densities, the VEs demonstrated a comparable pattern to the EEs, while CEs remained relatively stable across the various treaded PAN samples. Based on previous research **[23]**, improving the electrochemical reversibility of the vanadium redox reaction significantly contributes to the enhancement of VE and EE in the VFB single cell. As a result, cells equipped with thermally treated electrodes showcased greater charge and discharge capacities compared to cells utilizing untreated graphite felt.

The average CE, VE, and EE of the single cells, including the untreated and treaded rayon for 10 cycles at each current density are summarized in **Table** . The cells equipped with thermally treated rayon electrodes demonstrated superior discharge capacity and efficiencies compared to the untreated rayon. The thermal treatment conditions can be ranked in descending order of their average VE: 450 °C-3h (84%) > 450 °C-2h (83%) > 350 °C-2h (76%) > 250 °C-2h (73 %) > untreated (67%). The VRB cell employing rayon electrodes treated at a temperature of 450 °C for a duration of 3 hours exhibited remarkable performance and achieved the highest efficiencies in terms of EE (83%) and VE (84%). Likewise, the application of thermal treatment improves the efficiency at higher current density. In fact, the assembled cell containing untreated rayon electrodes are unable to withstand the C/D cycling at 200 mA/cm^2 for more than one cycle. Therefore, the efficiencies can't be calculated for the VFB at the higher current density for untreated rayon. However, through thermal treatment, the stability of the electrodes was enhanced, resulting in an increase in VE and EE to 70% and 69%, respectively for the 450 °C. The enhanced VE in the VFB cell employing the treated graphite felts arises from the easier and faster redox reactions, which is a result of reduced overpotential polarization. These results align with those findings obtained from CV and EIS measurements.

Based on the comparison of the C/D curves, the thermally treated samples exhibited significant improvements in efficiencies, like VE, EE, and CE. These improvements can be attributed to a decrease in the overpotential and a better use of the electrolyte, which can be explained by the following factors. First, thermal treatment causes an increase in the hydrophilic character of the graphite felt surface, making the active sites more accessible to the vanadium ions in the electrolyte. This change in the felts from hydrophobic to hydrophilic was confirmed through the wettability test depicted in **Figure 9**. Second, the number of oxygen-containing functional groups on the graphite felts surface was increased upon thermal treatment. As a result, a larger quantity of vanadium ions could effectively participate in parallel redox reactions, leading to more rapid and reversible electrochemical processes within the VFBs. The beneficial influence of the thermal treatment on the electrochemical performance was confirmed by the discernibly low charge transfer resistance measured by EIS and the remarkable reversibility observed during the CV measurements.

Table 7: Summary of VFB single-cell efficiencies, incorporating treated PAN electrodes at different current densities.

	Current density (mA/cm^2)	Coulombic efficiency (%)	Energy efficiency (%)	Voltage efficiency (%)	Discharge capacity (Ah/mol)
untreated	100	98.61	69.59	70.57	3351
	200	98.07	62.09	63.31	2222
400 °C-2h	100	98.51	73.64	74.75	1570
	200	98.90	64.90	65.62	2523
500 °C-2h	100	97.98	84.28	86.01	3305
	200	99.89	72.61	72.67	2675
600 °C-0.5h	100	99.08	86.26	87.05	3586
	200	99.40	74.67	75.12	3138
600 °C-1h	100	99.07	88.52	89.34	3677
	200	99.26	79.12	79.69	3414
600 °C-2h	100	98.89	88.17	89.16	3660
	200	99.34	78.53	79.05	3319

Table 8: Summary of VFB single-cell efficiencies, incorporating treated rayon electrodes at different current densities.

	Current density (mA/cm^2)	Coulombic efficiency (%)	Energy efficiency (%)	Voltage efficiency (%)	Discharge capacity (Ah/mol)
untreated	100	98.28	66.05	67.21	2750
	200	--	--	--	--
250 °C-2h	100	98.2	71.9	73.2	3465
	200	--	--	--	--
350 °C-2h	100	98.59	75.23	76.31	3276
	200	98.95	62.94	63.31	1665
450 °C-1h	100	98.27	80.23	83.13	3336
	200	98.52	69.64	70.69	2552
450 °C-2h	100	98.95	82.57	83.44	3541
	200	99.30	69.75	70.24	2890
450 °C-3h	100	98.76	83.04	84	3613
	200	98.93	69.42	70.18	2987

In a study conducted by Sun et al., it was discovered that the rate-limiting step in the mechanism of the vanadium redox reaction occurs during the transfer of an oxygen atom at the positive electrode (referred to as step 2 in **Figure 3 (a)**) **[14]**. This finding suggests that the presence of oxygen groups on the electrode surface plays a crucial role in determining the overall rate of the redox reactions. Consequently, a higher concentration of oxygen-containing functional groups on the electrode surface is expected to result in increased activity for the vanadium species reactions. Based on this hypothesis, the differences in the electrochemical performance under the treatment conditions may be attributed to the differences in the number of carbon-oxygen groups formed on the electrode surface. Therefore, the most significant improvement in cell efficiencies and electrochemical performance of the treated felts was observed under the conditions of 600 °C for 1 hour for PAN and 450 °C for 3 hours for rayon, as these conditions likely resulted in the highest concentration of oxygen-containing functional groups and surface area of the electrode material.

4. CONCLUSION AND FUTURE PERSPECTIVES

In conclusion, the thermal treatment of graphite felts (PAN and rayon) was evaluated. By subjecting the graphite felt electrodes to various temperatures and treatment times, the surface activity of the electrode material was enhanced through an increase in the concentration of oxygen functional groups on the carbon surface. The felts undergo thermal treatment at specific temperature ranges, with rayon ranging from 300 to 500 °C and PAN ranging from 450 to 600 °C. The weight loss of the felts as a function of time was measured to assess the treatment's impact. Visual observations showed noticeable colour changes in the graphite felt surface after thermal treatment, and wettability tests confirmed improved hydrophilicity, which is reflected as rapid absorption of water droplets. CV curves reveal that the I_a/I_c is closer to 1 and the ΔE_p is smaller after the treatment, illustrating an increase in the reversibility and electrochemical activity. Also, The negative half-reaction demonstrates improved kinetics and reduced hydrogen evolution reaction after thermal treatment. In addition, the redox reaction kinetics were improved by the reduction in the charge-transfer resistance obtained from the EIS measurements.

Based on the experimental results, the most significant improvements in electrochemical performance were achieved under specific treatment conditions, which were determined to be 600 °C for 1 hour for PAN and 450 °C for 3 hours for rayon. Overall, based on all the experimental findings, it is evident that the application of thermal treatment significantly boosts the electrochemical performance of the VFB when utilized as electrodes. This enhancement is supported by the results obtained from CV, EIS, and charge-discharge measurements. The thermal treatment introduces a considerable number of functional groups on the surface of the graphite felts, which are recognized as electrochemically active sites for the vanadium redox reaction. Furthermore, the increased presence of oxygen-containing functional groups on the surface enhances its hydrophilicity, thereby promoting favourable electrochemical reactions.

This work has identified specific treatment conditions that yield substantial enhancements in the electrochemical performance of graphite felts used as electrodes in VFBs. To translate these improvements observed at the laboratory scale into production scale, further developments are necessary to evaluate the scalability and compatibility of the thermal treatment process with large-scale production techniques. It is important to investigate the impact of thermal treatment on commercial-grade graphite felts and assess its feasibility for implementation in industrial VFB systems.

Future research endeavours could also delve deeper into the nature and composition of these functional groups. Techniques, such as X-ray photoelectron spectroscopy (XPS) or Fourier-transform infrared spectroscopy (FTIR) can be employed to identify the specific oxygen-containing groups and acquire a comprehensive understanding of their influence on electrochemical activity. Also, subsequent research may encompass prolonged C/D tests and accelerated aging studies to evaluate the long-term stability and durability of the treated electrodes. This will provide insights into the resilience and practical applicability of the thermal treatment approach in real-world VFB systems. In addition to thermal treatment, exploring synergistic approaches can lead to further advancements in electrode performance. Combining thermal treatment with other surface modification techniques, such as chemical functionalization or deposition of nanomaterials, has the potential to yield synergistic effects and enhance the overall performance and stability of VFB electrodes.

5. REFERENCES

[1] Bayeh, A. W., Kabtamu, D. M., Chang, Y. C., Wondimu, T. H., Huang, H. C., & Wang, C. H. (2021). Carbon and metal-based catalysts for vanadium redox flow batteries: a perspective and review of recent progress. Sustainable Energy & Fuels, 5(6), 1668-1707.

[2] Leung, P., Li, X., De León, C. P., Berlouis, L., Low, C. J., & Walsh, F. C. (2012). Progress in redox flow batteries, remaining challenges and their applications in energy storage. Rsc Advances, 2(27), 10125-10156.

[3] Ye, R., Henkensmeier, D., Yoon, S. J., Huang, Z., Kim, D. K., Chang, Z., & Chen, R. (2018). Redox flow batteries for energy storage: a technology review. Journal of Electrochemical Energy Conversion and Storage, 15(1), 010801.

[4] Kim, K. J., Kim, Y. J., Kim, J. H., & Park, M. S. (2011). The effects of surface modification on carbon felt electrodes for use in vanadium redox flow batteries. Materials Chemistry and Physics, 131(1-2), 547-553.

[5] Kim, S. (2019). Vanadium redox flow batteries: electrochemical engineering. Energy Storage Devices, 1-19.

[6] Eifert, L., Banerjee, R., Jusys, Z., & Zeis, R. (2018). Characterization of carbon felt electrodes for vanadium redox flow batteries: impact of treatment methods. Journal of The Electrochemical Society, 165(11), A2577.

[7] Chen, R., Kim, S., & Chang, Z. (2017). Redox flow batteries: fundamentals and applications. Redox: Principles and Advance Applications, 103-118.

[8] Fink, H., Friedl, J., & Stimming, U. (2016). Composition of the electrode determines which half-cell's rate constant is higher in a vanadium flow battery. The Journal of Physical Chemistry C, 120(29), 15893-15901.

[9] Zhong, S., Padeste, C., Kazacos, M., & Skyllas-Kazacos, M. (1993). Comparison of the physical, chemical and electrochemical properties of rayon-and polyacrylonitrile-based graphite felt electrodes. Journal of Power sources, 45(1), 29-41.

[10] Pezeshki, A. M., Clement, J. T., Veith, G. M., Zawodzinski, T. A., & Mench, M. M. (2015). High performance electrodes in vanadium redox flow batteries through oxygen-enriched thermal activation. Journal of Power Sources, 294, 333-338.

[11] SGL-Carbon. (2023). SIGRACELL® Battery Felts. Retrieved from link.

[12] Rabbow, T. J., Trampert, M., Pokorny, P., Binder, P., & Whitehead, A. H. (2015). Variability within a single type of polyacrylonitrile-based graphite felt after thermal treatment. Part I: physical properties. Electrochimica Acta, 173, 17-23.

[13] Oriji, G., Katayama, Y., & Miura, T. (2005). Investigations on V (IV)/V (V) and V (II)/V (III) redox reactions by various electrochemical methods. Journal of Power Sources, 139(1-2), 321-324.

[14] Sun, B., & Skyllas-Kazacos, M. (1992). Modification of graphite electrode materials for vanadium redox flow battery application—I. Thermal treatment. Electrochimica acta, 37(7), 1253-1260.

[15] Park, S. K., Shim, J., Yang, J. H., Jin, C. S., Lee, B. S., Lee, Y. S., & Jeon, J. D. (2014). The influence of compressed carbon felt electrodes on the performance of a vanadium redox flow battery. Electrochimica Acta, 116, 447-452.

[16] Lindner, A., Radinger, H., Scheiba, F., & Ehrenberg, H. (2022). Structure–activity correlation of thermally activated graphite electrodes for vanadium flow batteries. RSC advances, 12(22), 14119-14126.

[17] Zhou, X. L., Zeng, Y. K., Zhu, X. B., Wei, L., & Zhao, T. S. (2016). A high-performance dual-scale porous electrode for vanadium redox flow batteries. Journal of Power Sources, 325, 329-336.

[18] Vanadium redox flow batteries with different electrodes and membranes. World J. Chem. Educ, 6(1), 8-13.

[19] Azpitarte, I., Eletxigerra, U., Barros, A., Aranzabe, E., & Cid, R. (2023). Electrochemical Evaluation of Different Graphite Felt Electrode Treatments in Full Vanadium Redox Flow Batteries. Batteries, 9(1), 39.

[20] Zhu, H. Q., Zhang, Y. M., Yue, L., Li, W. S., Li, G. L., Shu, D., & Chen, H. Y. (2008). Graphite–carbon nanotube composite electrodes for all vanadium redox flow battery. Journal of Power Sources, 184(2), 637-640.

[21] Zhang, L., Yue, J., Deng, Q., Ling, W., Zhou, C. J., Zeng, X. X., & Wu, Y. (2020). Preparation of a porous graphite felt electrode for advance vanadium redox flow batteries. RSC advances, 10(23), 13374-13378.

[22] Taylor, S. M., Pătru, A., Fabbri, E., & Schmidt, T. J. (2017). Influence of surface oxygen groups on V (II) oxidation reaction kinetics. Electrochemistry Communications, 75, 13-16.

[23] Mazúr, P., Mrlík, J., Beneš, J., Pocedič, J., Vrána, J., Dundálek, J., & Kosek, J. (2018). Performance evaluation of thermally treated graphite felt electrodes for vanadium redox flow battery and their four-point single cell characterization. Journal of Power Sources, 380, 105-114.